The Vertical Profile of Wind and Temperature in Cyclones and Anticyclones over the Eastern Two-Thirds of the United States: A Climatology

HOWARD B. BLUESTEIN AND PETER C. BANACOS*

School of Meteorology, University of Oklahoma, Norman, Oklahoma

(Manuscript received 7 December 2000, in final form 4 September 2001)

ABSTRACT

A climatological analysis, based upon operational surface and upper-air data from 1957 to 1994, of the wind and temperature profiles composited with respect to each quadrant of surface cyclones and anticyclones, is presented for the eastern two-thirds of the United States. The cyclones and anticyclones are located via an objective procedure. Hodographs and soundings are also composited with respect to season, geographic region, time of day, and, for cyclones only, intensity. Vertical profiles of the static-stability parameter are composited with respect to season and quadrant for both cyclones and anticyclones. The structures of mean cyclones and anticyclones are shown and discussed.

A diurnal variation in hodographs (vertical shear) is found, which shows up in both cyclones and anticyclones as a rotation in the counterclockwise direction between 0000 and 1200 UTC above the boundary layer. The effect is greater in cyclones than in anticyclones. This variation is hypothesized to be in part due to a tidal oscillation and in part due to radiative–thermal effects.

In the mean, a well-pronounced equatorward-directed low-level jet is resolved in the northwest quadrant of surface cyclones. Low-level jets do not show up in the mean in other quadrants of cyclones or in anticyclones. The curvature of hodographs near the tropopause is clockwise in cyclones and counterclockwise in anticyclones.

1. Introduction

Climatological analyses of extratropical synoptic-scale systems have, up to recently, documented the frequency, tracks, and preferred regions of cyclogenesis, cyclolysis, anticyclogenesis, and anticyclolysis in both the Northern (e.g., Petterssen 1956; Taylor 1986; Zishka and Smith 1980; Whittaker and Horn 1984) and Southern (e.g., Taljaard 1967; Sinclair 1994) Hemispheres. The interannual variability of cyclone frequency (Changnon et al. 1995) and the climatology of meteorological ''bombs'' (Sanders and Gyakum 1980) are examples of other more specialized investigations. However, the authors are unaware of climatological assessments of how the thermodynamic and vertical-shear profiles of baroclinic, extratropical disturbances vary within their synoptic-scale, parent disturbances.

A climatological assessment of the theromodynamic and vertical-shear profiles is important for several reasons. First, the nature of a number of mesoscale systems depends on them. For example, the nature of convective-scale and mesoscale precipitation systems embedded within synoptic-scale features depends upon the wind and temperature structure of their parent system. In the last 20 years we have learned, from numerical simulation experiments (e.g., Weisman and Klemp 1982, 1984), theory (e.g., Rotunno and Klemp 1982, 1985), and observations (e.g., Maddox 1976; Bluestein and Jain 1985), how the nature of convective storms is related to the convective available potential energy and to the vertical-shear profile. We have also learned how the mesoscale organization of stratiform precipitation systems, particularly banded precipitation in the vicinity of frontal zones embedded in extratropical cyclones, is related to the temperature, moisture, and vertical-shear profiles (e.g., Wolfsberg et al. 1986; Schultz and Schumacher 1999).

In addition, local maxima (with respect to height) in wind speed at low levels have been documented in the poleward airstream ahead of surface cyclones (Bluestein 1993, p. 390) and in the equatorward airstream behind surface cyclones (Bluestein 1993, p. 391). The former often play a role in transporting warm, moist air poleward and the latter often play a role in transporting cold, dry air equatorward. The authors are unaware of any long-term climatologies of these low-level jets.

In recent years compact disc technology has allowed us to access easily large meteorological datasets (Mass

* Current affiliation: NOAA/NWS/NCEP/Storm Prediction Center, Norman, Oklahoma.

Corresponding author address: Dr. Howard B. Bluestein, School of Meteorology, University of Oklahoma, 100 E. Boyd, Rm. 1310, Norman, OK 73019.
E-mail: hblue@ou.edu

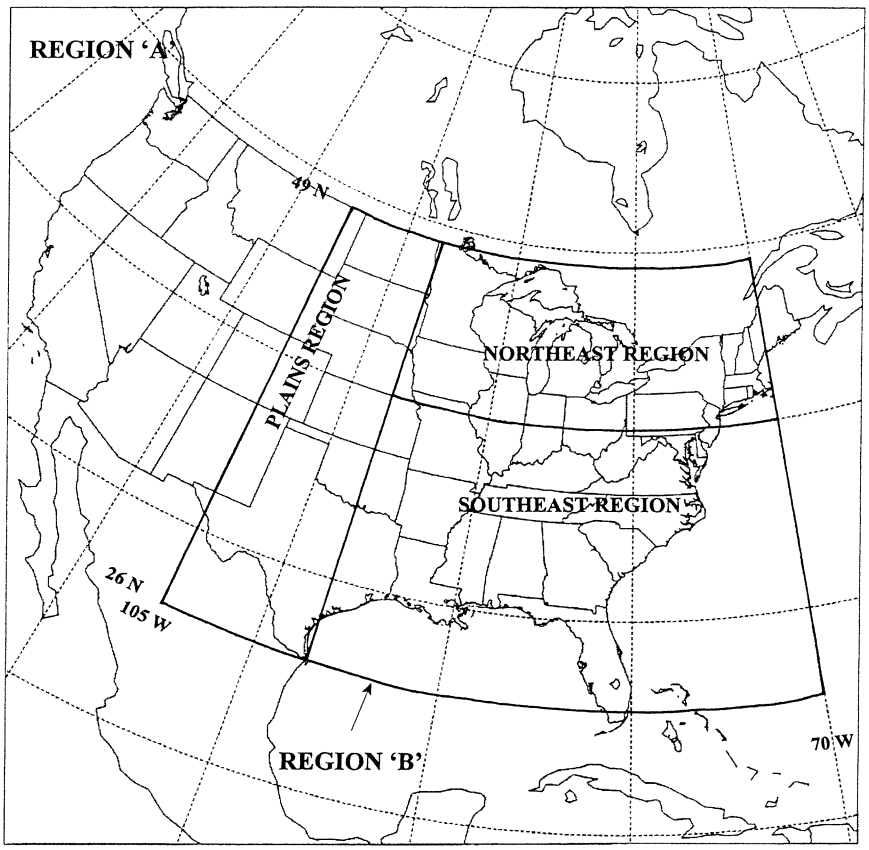

FIG. 1. The region of the Western-Northern Hemisphere in which surface cyclones and anticyclones were objectively located (region A). Cyclones and anticyclones only within region B were considered in composites. Soundings for composites to be described later came from region B and the area just outside region B (i.e., within 500 km of the cyclone and anticyclone centers in region B).

et al. 1987; Mass 1993); in addition, large datasets archived on mass-storage devices are easily available over the Internet. It is therefore appropriate now to compile a climatology of the vertical profile of wind and temperature in synoptic-scale, extratropical cyclones and anticyclones. The purpose of this paper is to present and discuss the implications of such climatological analyses, with an emphasis on the seasonal and diurnal variations, and to a lesser extent on regional variations. The focus of this study is on systems in the central and eastern sections of the United States. We believe that our study is unique in that the results are valid in a reference frame moving with cyclones and anticyclones themselves, instead of in a reference frame fixed with respect to the ground as has been done before [e.g., Wallace and Hartranft (1969) examined the diurnal wind variation in a ground-based reference frame].

In section 2, the data sources and methodology of processing the data are detailed. Climatologies of surface cyclones and anticyclones are presented and discussed in section 3. Climatological analyses of hodographs are presented in section 4 and corresponding analyses of thermal structure are shown in section 5. In section 6, mean cross sections of wind and potential temperature through cyclones and anticyclones are presented and discussed. Section 7 contains a summary and discussion of the results and suggestions for further studies.

2. Data and methodology of data processing

a. Strategy for locating surface cyclones and anticyclones

We first compiled an objective climatology of the locations of the centers of surface cyclones and anticyclones over a broad area covering all of the United States and nearby surrounding regions (Fig. 1). The climatology is based on sea level pressure data from twice-daily (0000 and 1200 UTC) hemispheric, gridded analyses from version III of the National Meteorological Center [NMC, now known as the National Centers for Environmental Prediction (NCEP)]–National Center for Atmospheric Research (NCAR) hemispheric gridpoint data archive from 1946 to 1994. These data, stored on the NMC octagonal (polar stereographic) grid (with

381-km grid spacing at 60°N) were obtained from a set of two compact discs from the Department of Atmospheric Sciences at the University of Washington (Mass et al. 1987; Mass 1993). The analyses in this dataset come from those done by the United States Navy for 1946–93 and from NMC ''final analyses'' for 1994 (i.e., although the dataset is from the NMC–NCAR archive, the surface dataset was mostly produced by the U.S. Navy). The U.S. Navy's operational analysis system has evolved in a similar fashion to that of other operational forecasting centers (e.g., Dey 1989) while employing largely the same observational data sources (Goerss and Phoebus 1992). The navy changed from a successive corrections technique to a global multivariate optimum interpolation analysis beginning in 1988 (Barker 1992), and new preanalysis objective quality control procedures were also implemented that year (Baker 1992). Since these analyses were used as part of a data assimilation procedure for running the Navy Operational Global Atmospheric Prediction System (NOGAPS) model, which became operational in 1982 (Rosmond 1992), it is expected that the redistribution of sea level pressure is influenced to some degree by model-related processes, especially in later years of the analysis period. During the early years of our dataset (1946–75) a ''fields of information blending'' (FIB) technique developed by M. Holl at the Naval Research Laboratories (NRL)/Fleet Numerical Meteorology and Oceanography Center (FNMOC) was used to generate the sea level pressure analyses (P. Pauley 2001, personal communication). This methodology involved the use of an iterative weak-constraint variational analysis of a recent numerical forecast and a previous analysis. Some version of the FIB analysis was used for sea level pressure until the multivariate optimum interpolation scheme was implemented in 1988 and used through the end of our dataset. So, all the sea level pressure analyses were affected by model processes to some extent.

Missing analyses had been replaced by analyses from the air force, NMC operational and ''final'' hemispheric analyses, and ongoing research projects. Subjective surface analyses had been digitized manually and included as part of the record, especially for data through the end of the 1950s. From 1946 to 1954, and for shorter intermittent periods between 1960 and 1962, analyses were available just once daily at 1200 UTC.

Since the dataset was not homogeneous over the entire 1946–94 period, it is possible that there might be different biases during some periods, owing to the different analysis procedures, which have not been documented very well; however, we did not think it worthwhile to standardize and reanalyze the entire dataset ourselves, which would have been an overwhelming task. It was also decided not to use the recently completed NCEP–NCAR reanalysis project data (Kalnay et al. 1996) mainly because it was not available at the outset of this study. (In addition, it was felt that it would be best initially to use analyses mainly of observational data, which are not affected by model-related processes such as the parameterization of latent heat release. However, we did accept the use of the sea level pressure data from the navy, which were in fact affected by model processes. The upper-air dataset, to be discussed later, were in fact collected from real observations, not from model-affected fields.)

For the purpose of quality control, each set of gridded data was inspected; grossly corrupted analyses were discarded. In addition, each month we compared a random subset of the surface pressure analyses with analyses from the *Daily Weather Maps* series published by the United States Department of Commerce. On the basis of our comparisons, it was concluded that the evolution of operational objective analysis methodology did not impact the synoptic-scale sea level pressure analyses significantly in a qualitative sense.

In order to locate cyclones and anticyclones more precisely (but not necessarily more accurately), we reanalyzed the data from the relatively coarse NMC grid onto a polar stereographic grid having the same corner points, and exactly half the spacing of a 256-point subset of the NMC grid (Fig. 1, region A). We used a three-pass Barnes (1964) scheme largely following the guidelines of Koch et al. (1983); the scheme was configured so that the rms difference between the initial and collocated analysis points was on the order of 0.2 mb, which is very small compared to the amplitude of the pressure variations in cyclones and anticyclones.

Errors in determining the locations of cyclones and anticyclones from a discrete set of points are from spatial-truncation errors (Changnon et al. 1995) and lack of sufficient resolution. Lack of spatial resolution did not allow us to determine accurately the value of the pressure extremum at the center of the most intense pressure systems. For most extratropical systems, however, the difference between the subjectively estimated pressure extremum (determined from the *Daily Weather Map* series) and the objectively determined extremum was not greater than 3–4 mb. Dickinson et al. (1997) found a slightly greater difference (5 mb) between the NMC gridded sea level central pressure and the NMC subjective surface analysis central pressure in an intense cyclone over the Gulf of Mexico.

The objective procedure for locating pressure systems from the reanalyzed data involved first identifying grid points having a sea level pressure less than 1000 mb for cyclones and greater than 1026 mb for anticyclones. The threshold value in cyclones was chosen subjectively; the threshold value for anticyclones was chosen to be 13 mb greater than standard atmosphere sea level pressure to be consistent with the 13-mb pressure-deficit (with respect to standard atmosphere sea level pressure) threshold in cyclones. The use of these threshold values for cyclones and anticyclones may exclude weak cyclones and anticyclones, especially during the summer, but include many weak cyclones and anticyclones, especially during the winter. Thus the dataset may be bi-

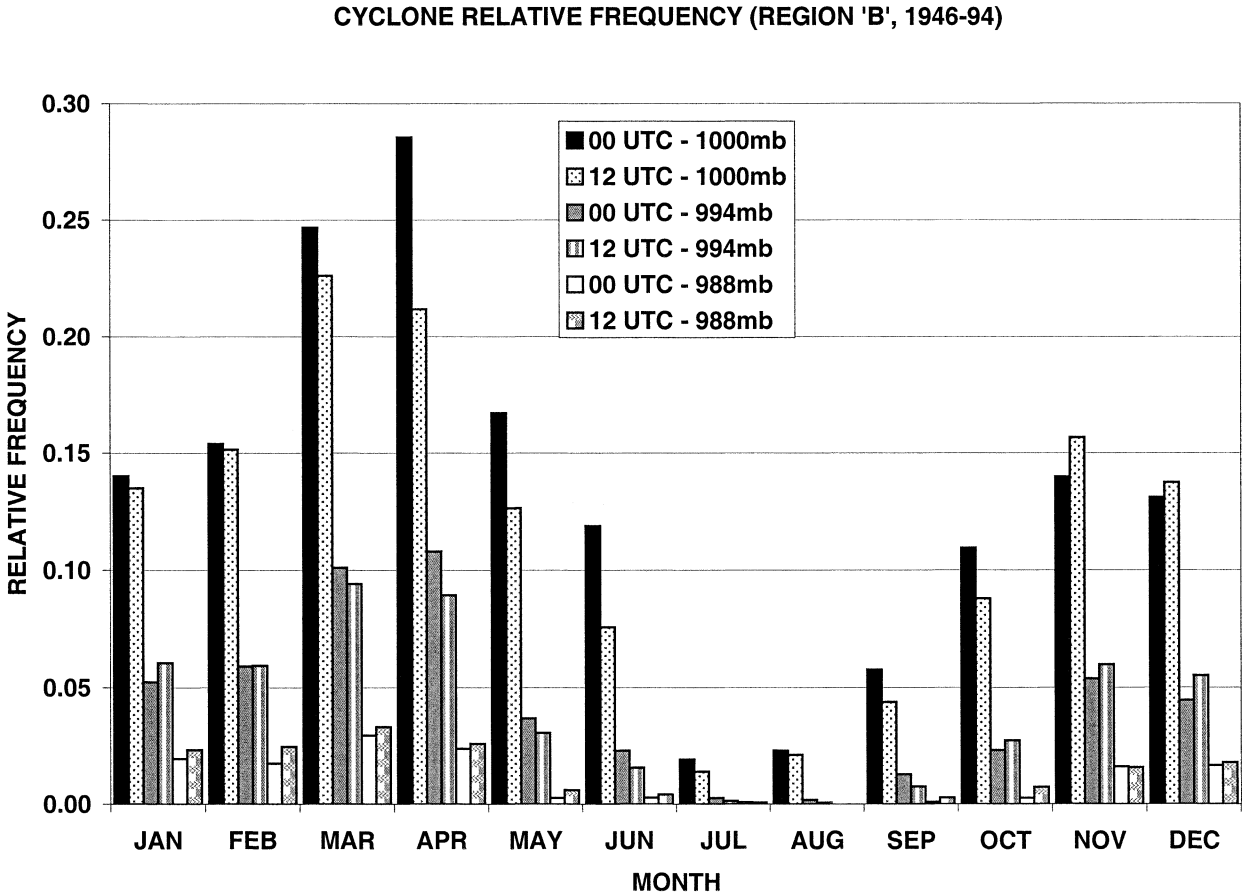

FIG. 2. Relative frequency of synoptic-scale, extratropical (a) cyclones and (b) anticyclones over the eastern two-thirds of the United States from 1946 to 1994 by month and time (0000 and 1200 UTC). "Relative frequency" is the number of systems meeting the objective criteria described in the main body of the paper divided by the number of map times.

ased toward stronger systems during the summer and weaker systems during the winter. To see how sensitive climatologies are to threshold values, cyclones were also located for threshold values of 994 and 988 mb and anticyclones were also located for threshold values of 1032 and 1038 mb, that is, for deviations of 6 and 12 mb from the other thresholds. Systems within one grid point of the edge of the boundaries in Fig. 1 were not considered. Since elongated surface pressure troughs and ridges do not have well-defined centers, we excluded them by imposing the following isobar-circularity criteria: For both cyclones and anticyclones,

$$|\partial^2 p/\partial x^2| \quad \text{and} \quad |\partial^2 p/\partial y^2| > 1/3.3|\nabla^2 p|.$$

The circularity criteria were chosen subjectively. Elongated Arctic anticyclones east of the Rockies and weak cyclones along frontal boundaries are not generally captured. However, a sample composed of more circular systems is better suited for the quadrant-averaging approach used to examine their structure. If a system were identified in an analysis, any additional one had to be at least 1500 km (approximately one-half wavelength of most synoptic-scale, extratropical systems) away from the previously identified one, in order to be certain it was truly a separate system.

Since the object of our study is extratropical systems, tropical warm-core systems near shore were excluded from the sample. Tropical warm-core systems were identified from 6-h Atlantic tropical cyclone data compiled by the National Hurricane Center; 113 cases were removed from the sample. Since the locations of tropical systems over the ocean are usually known more accurately than those of their extratropical counterparts, owing to satellite, operational weather radar, and in situ reconnaissance aircraft observations, it was possible to determine the differences between the actual tropical cyclone locations and the estimates based on the reanalyzed gridded data. We were therefore able to estimate the spatial errors involved in determining system location by our procedure. In conjunction with other quality control procedures based on the rawinsonde data (cf. section 2b), these spatial errors do not affect our results appreciably. The mean difference in location was 86 km, which is less than the average difference between surface observing sites over land and 25% of the average spacing between rawinsonde sites. Since extratropical

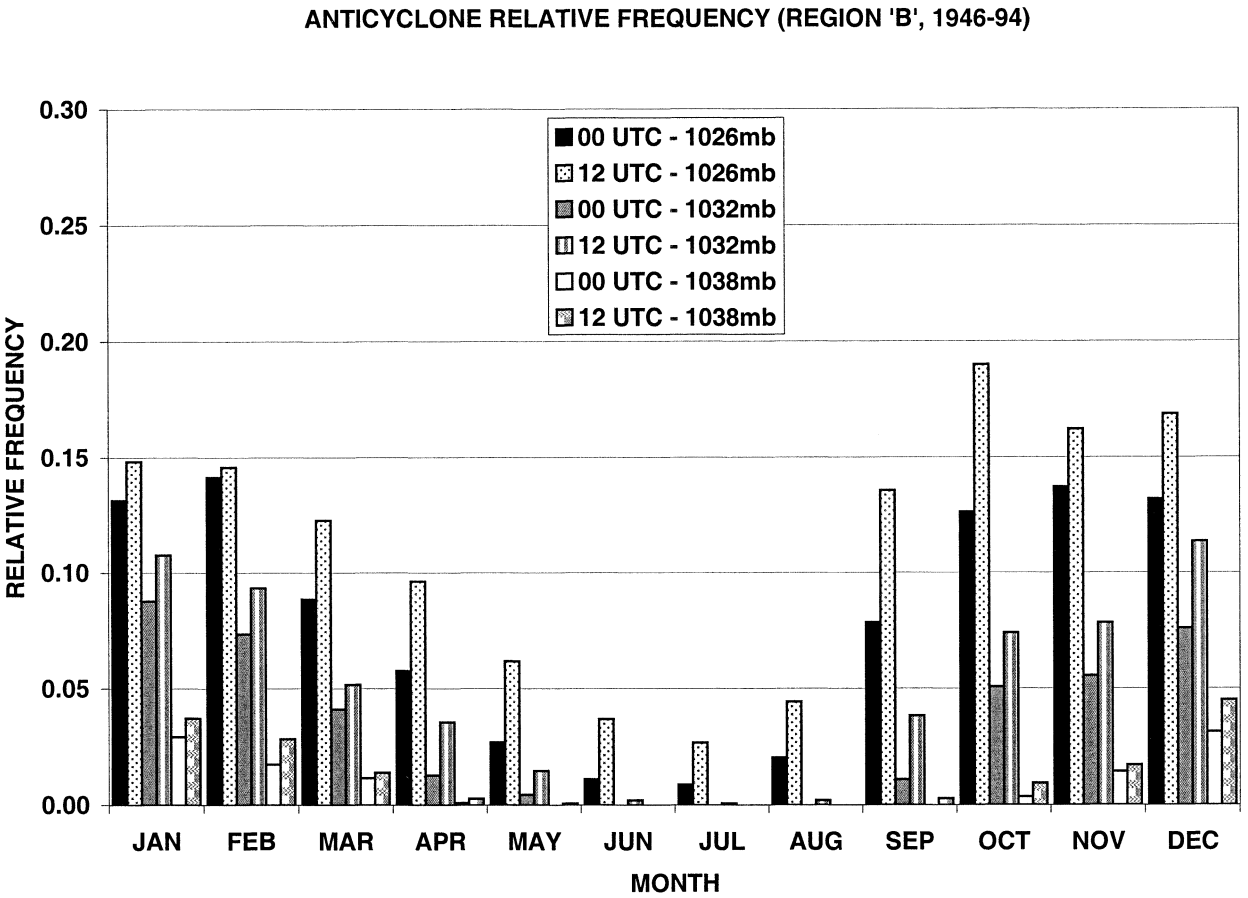

FIG. 2. (*Continued*)

systems tend to be broader than tropical systems, the locations of them over land are probably known with even better accuracy.

Altogether, 31 082 NMC grids were analyzed over the 49-yr period from 1946 to 1994. In the eastern two-thirds of the United States and adjacent portions of Canada, the Gulf of Mexico, and the Atlantic Ocean (Fig. 1, region B), 3808 (nontropical) cyclones and 3040 anticyclones were identified. Since 57% of the grid times were at 1200 UTC, these statistics could be biased toward systems more prevalent at that time of day. Any significant differences could be a result of diabatic processes or topography. The overall relative frequency of occurrence of cyclones was 0.1225, or roughly one cyclone every 8 maps; it is greater than the relative frequency of occurrence of anticyclones, which was 0.0978, or roughly one anticyclone every 10 maps. (Our counting procedure does not identify independent cyclones; i.e., the same cyclone appearing on a sequence of maps does not count as one cyclone. The relative frequency of occurrence of cyclones is the number of cyclones on each map meeting the central pressure criterion divided by the number of individual maps used.) Although we did not compute a climatology that included weaker systems, it is obvious that one would exhibit a much higher frequency of occurrence of cyclones and anticyclones. It is recognized that central pressure is not necessarily an indication of intensity; for example, during the winter a cyclone may be relatively intense (i.e., the magnitude of the horizontal pressure gradient is intense), even when its central pressure is not relatively low.

b. Strategy for compositing hodographs and thermodynamic soundings

Rawinsonde data from 1946 to 1994 that had been archived by the National Weather Service and the military were obtained, for North America, from the National Climatic Data Center (NCDC). Owing to a different standard time for balloon launches before 1 June 1957, we decided to consider data only from 1 June 1957 to 31 December 1994 for this portion of the study. It was still possible to obtain a large statistical sample from this subset of all the data available.

Data from all rawinsonde launches within 500 km (less than a quarter wavelength of most systems) of the center of surface pressure systems in the eastern two-thirds of the United States and adjacent regions were compiled and the quadrant (northeast, southeast, south-

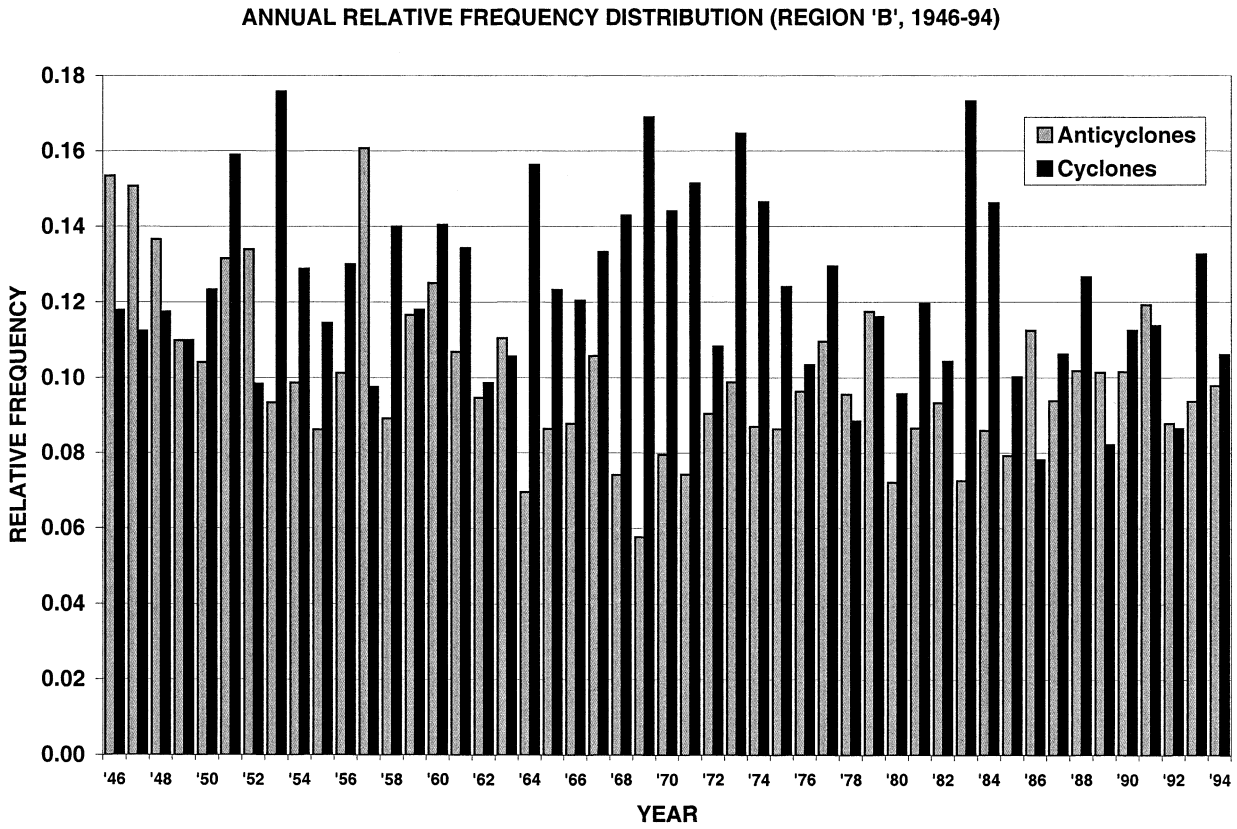

FIG. 3. Relative frequency of synoptic-scale, extratropical cyclones and anticyclones from 1946 to 1994, by year.

west, and northwest) relative to the center of each system was noted. We did not consider data from the western one-third of the United States because the complex terrain there makes interpretation of the data more difficult and even impossible in areas of very high terrain.

The dataset is not homogeneous over the duration of the sample because instruments and operating procedures have undergone changes (Friedman 1972; Pratt 1985), there have been some flawed automated processing procedures (Schwartz 1990), the network has undergone changes (Bosart 1990; Elliott and Gaffen 1991), and the equipment is not uniform (Schwartz and Doswell 1991). However, the various problems with operational rawinsonde data have been well documented in the literature.

To address these problems prior to compiling the data, several objective and subjective quality control measures were implemented to eliminate superadiabatic layers and supersaturated levels. In addition, height data computed above the highest level for which temperature data were available were discarded in order to avoid hydrostatic inconsistencies (Gandin 1988; Collins and Gandin 1990).

Because there is an uncertainty about the precise location of the center of surface systems, we imposed an additional check on the rawinsonde-site quadrants relative to the center of the systems when they were within 250 km of the center of surface systems and when the surface wind was in excess of 5 m s^{-1}. We made sure that the observed wind direction was within 90° of the wind direction estimated from the geostrophic wind modified by a 30° cross-isobar (toward lower pressure) component to account for friction and baroclinicity (Hoxit 1974). In rare instances when the surface wind direction did not satisfy this constraint, the wind observation was relocated to the quadrant in which it was satisfied.

We then imposed a statistical quality control on the data by checking manually all data that were three or more standard deviations from the seasonal and quadrant means. If these data were associated with an extreme event, they were retained; otherwise, if they lacked spatial and/or temporal coherence (i.e., if they were grossly unrepresentative as a result of instrument or other problems), they were discarded. We anticipate that by careful quality control procedures and examining a very large data sample, these problems will not significantly affect our results.

3. Climatology of surface cyclones and anticyclones

Over the 49-yr period from 1946 to 1994 surface cyclones (anticyclones) in the eastern two-thirds of the United States were more common at 0000 (1200 UTC)

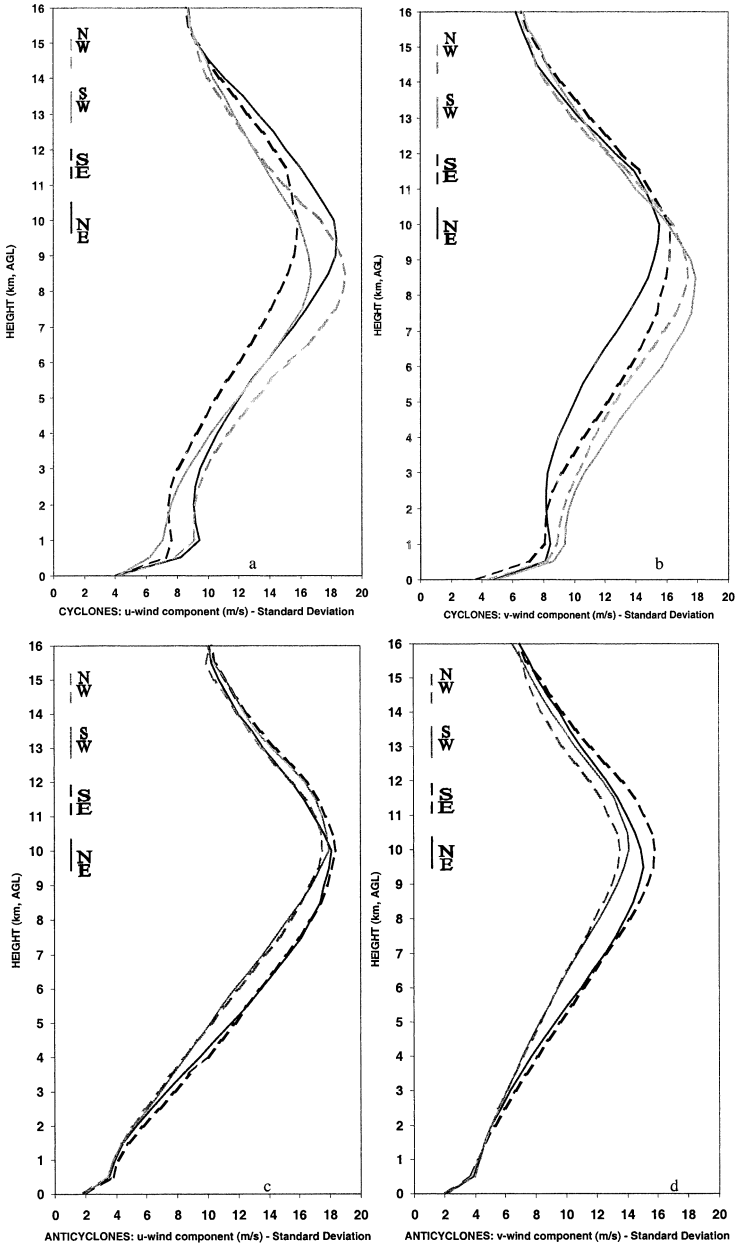

FIG. 4. Std dev, as a function of height (km AGL), in the northeast (dark solid line), southeast (dark dashed line), southwest (light solid line), and northwest (light dashed line) quadrants (within 500 km of the centers) of (a) the zonal (u) component of the wind in cyclones, (b) the meridional (v) component of the wind in cyclones, (c) the zonal component of the wind in anticyclones, and (d) the meridional component of the wind in anticyclones.

than at 1200 (0000 UTC) (Fig. 2) when anticyclones whose central pressure exceeded any of the three thresholds were counted, but only when cyclones whose central pressure was below 1000 mb were counted; when the threshold pressure for cyclones was decreased to 994 and 988 mb, cyclones were found to be more common at 0000 UTC than 1200 UTC mainly during the spring (March–June) and early fall (September) only. During the fall and early winter (October–January), the deeper (994-mb threshold) cyclones were more common at 1200 UTC than 0000 UTC. The deepest cyclones (988-mb threshold), on the other hand, were more common at 1200 UTC than 0000 UTC for most of the year. The opposite diurnal behavior of cyclone and anticyclone frequency of occurrence when the cyclones and anticyclones were relatively weak can be explained as

TABLE 1. Number of soundings used in each composite.

Composite type	NE quadrant	SE quadrant	SW quadrant	NW quadrant
All cyclones	3182	4183	3890	3112
0000 UTC	1687	2228	1981	1635
1200 UTC	1495	1955	1909	1477
All anticyclones	2853	3259	3271	2815
0000 UTC	1075	1226	1275	1179
1200 UTC	1778	2033	1996	1636
Spring cyclones	1439	1822	1663	1367
0000 UTC	790	996	882	722
1200 UTC	649	826	781	645
Summer cyclones	268	427	327	276
0000 UTC	162	253	182	168
1200 UTC	106	174	145	108
Fall cyclones	570	843	772	562
0000 UTC	286	452	384	292
1200 UTC	284	391	388	270
Winter cyclones	905	1093	1131	908
0000 UTC	451	529	536	454
1200 UTC	454	564	595	454
Spring anticyclones	528	554	625	516
0000 UTC	176	176	228	201
1200 UTC	352	378	397	315
Summer anticyclones	145	225	225	160
0000 UTC	35	56	54	48
1200 UTC	110	169	171	112
Fall anticyclones	1101	1285	1242	1039
0000 UTC	416	465	480	414
1200 UTC	685	820	762	625
Winter anticyclones	1083	1203	1183	1103
0000 UTC	449	532	515	518
1200 UTC	634	671	668	585
Northeast region cyclones	1174	1754	1845	957
0000 UTC	532	833	847	445
1200 UTC	642	921	998	512
Southeast region cyclones	596	524	676	877
0000 UTC	296	263	335	442
1200 UTC	300	261	341	435
Plains region cyclones	1410	1905	1370	1281
0000 UTC	861	1133	801	750
1200 UTC	549	772	569	531
Northeast region anticyclones	1120	1548	1588	938
0000 UTC	420	581	613	381
1200 UTC	700	967	975	557
Southeast region anticyclones	1313	1048	1155	1409
0000 UTC	490	382	449	601
1200 UTC	823	666	706	808
Plains region anticyclones	426	664	530	474
0000 UTC	169	264	214	199
1200 UTC	257	400	316	275
Cyclones, $p_{min} < 980$ mb	36	69	58	47
Cyclones, $\zeta_g > 2f$	320	363	356	362
Cyclones, $\zeta_g > 3f$	39	26	46	49
Albany, NY, cyclones				
0000 UTC	28	52	61	25
1200 UTC	21	48	39	33
Green Bay, WI, cyclones				
0000 UTC	59	52	95	31
1200 UTC	92	54	119	38
Oklahoma City, OK, cyclones				
0000 UTC	34	72	18	10
1200 UTC	18	76	16	8
Greensboro, NC, cyclones				
0000 UTC	14	19	23	20
1200 UTC	13	17	28	14

TABLE 1. (*Continued*)

Composite type	NE quadrant	SE quadrant	SW quadrant	NW quadrant
Albany, NY, anticyclones				
0000 UTC	41	43	30	27
1200 UTC	98	53	69	34
Green Bay, WI, anticyclones				
0000 UTC	53	27	31	22
1200 UTC	60	42	48	39
Oklahoma City, OK, anticyclones				
0000 UTC	2	19	13	12
1200 UTC	13	22	17	21
Greensboro, NC, anticyclones				
0000 UTC	15	38	45	38
1200 UTC	53	103	71	22

a hydrostatic consequence of radiative cooling during the night (higher surface pressure in the early morning) and insolational heating during the day (lower surface pressure late in the afternoon). When cyclones are deeper, they may be overall more intense, so that the magnitude of the surface pressure gradient is stronger, the surface winds stronger, and the effects of vertical mixing in the boundary layer more intense; the effect of the latter might be to reduce the effects of radiative temperature changes.

Cyclones were most common in late winter and early spring, and least common in the summer (Fig. 2a), when there is the least pole-to-equator baroclinicity over the United States; there was a relative maximum in frequency of occurrence in late fall and a relative minimum during midwinter when the pressure threshold was 1000 and 994 mb, but not when the pressure threshold was decreased to 988 mb. The midwinter relative minimum is probably a result of the inhibition of baroclinic instability due to high static stability at low levels over the North American continent and likely does not occur with extratropical oceanic cyclones. Anticyclones were most common during the fall, relatively frequent during the winter, and least frequent during the summer (Fig. 2b).

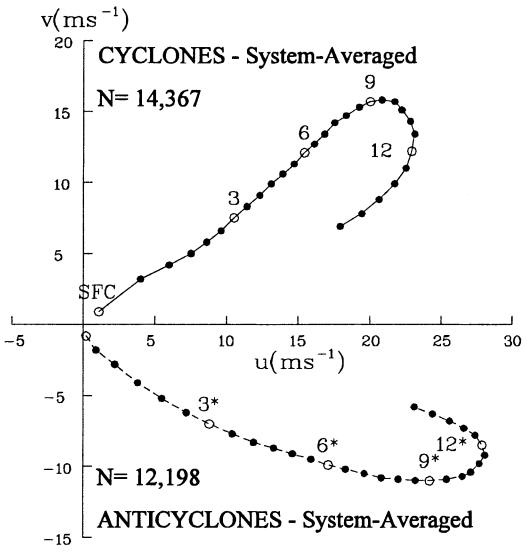

FIG. 5. Composite hodographs for region B of Fig. 1, for 1 Jun 1957–31 Dec 1994, for all cyclones (solid line) and all anticyclones (dashed line) regardless of quadrant. Numbers plotted are heights in km AGL. The sample size (*N*) of each composite is indicated in each panel; first (second) number is for the solid-line (dashed-line) cases.

The annual relative frequencies of cyclones and anticyclones (Fig. 3) exhibit large year-to-year variability. From Fig. 3 it may be inferred that there could be a slight trend of decreasing cyclone frequency over the period of record, as has also been noted by Changnon et al. (1995). It is beyond the scope of this paper to discuss or explain this finding, other than to note that we have independently supported their results. The spatial distributions of cyclones and anticyclones over the 49-yr period (not shown) are generally consistent with the climatologies of Whitaker and Horn (1984) and Zishka and Smith (1980), even though their studies may have included weaker systems. The similarities between our climatologies of surface cyclones and anticyclones with those independently formulated by others is additional confirmation that our objective techniques for locating surface cyclones and anticyclones are effective.

4. Climatological analyses of hodographs

Table 1 lists the number of soundings used to prepare each composite hodograph. For most composites, hundreds of soundings were used; in many instances well in excess of a thousand soundings were used. In the worst case, summertime anticyclones at 0000 UTC, only several dozen soundings were used.

Wind composites were computed by averaging the zonal and meridional components separately, as has been done in another context by Carr and Millard (1985). Owing to the ''nonuniqueness'' of vector interpolation (Schaefer and Doswell 1979), the magnitude of the averaged winds is less than the average wind speed in each composite. The composite hodographs were calculated from data interpolated at 500-m inter-

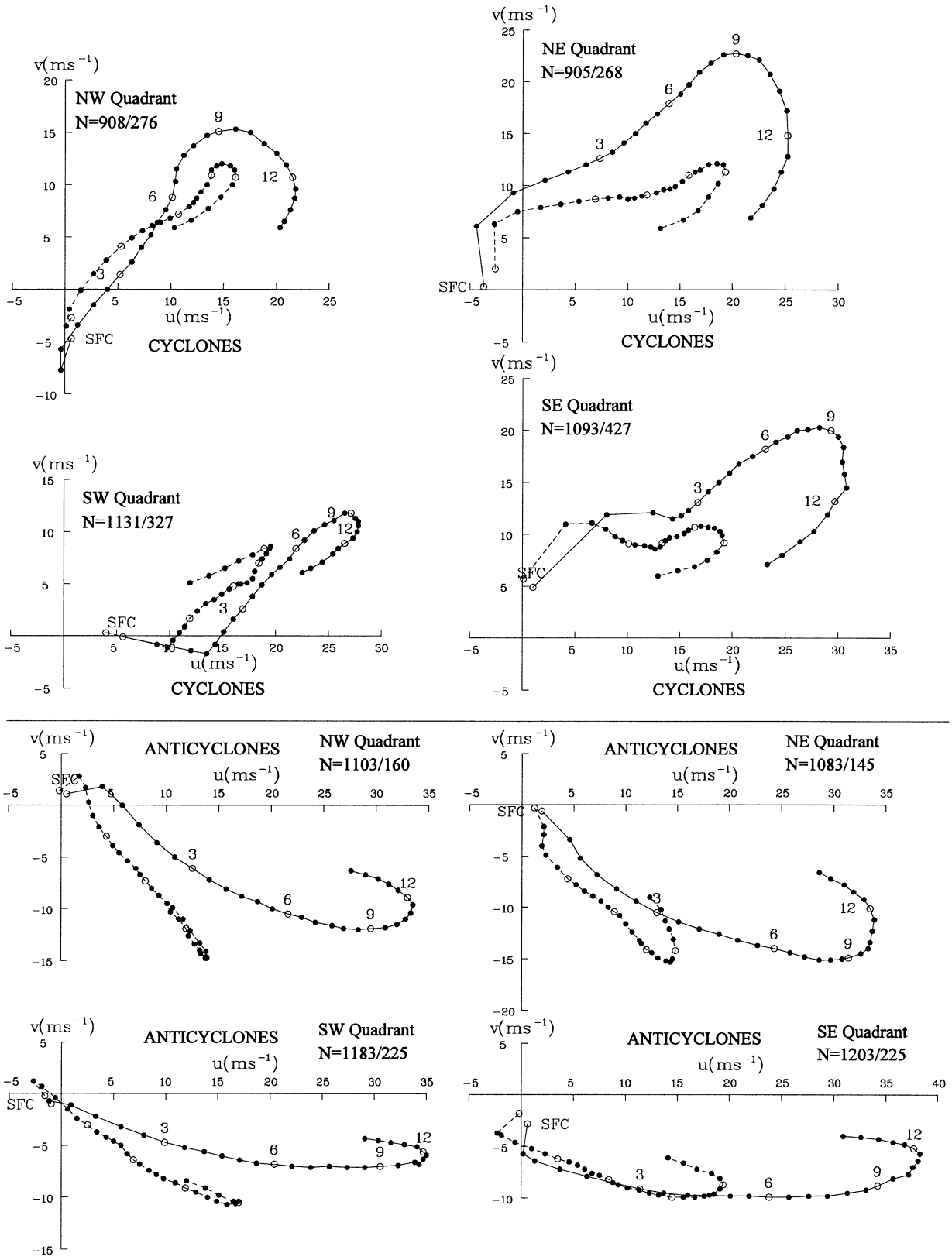

FIG. 6. As in Fig. 5 but for each quadrant of surface (top) cyclones and (bottom) anticyclones for winter (solid line) and summer (dashed line). Winter and summer seasons are Dec–Feb and Jun–Aug, respectively.

vals AGL. The composite data were interpolated to height AGL in order to represent the boundary layer properly. [Composites interpolated with respect to pressure (not shown) were not significantly different at upper levels from those interpolated with respect to height AGL.] None of the composite hodographs were subject to any additional smoothing in the vertical; all composite hodographs were calculated from raw averages.

a. Variability of winds with height

Before we discuss the composite hodographs by quadrant for each season, it is useful to see how the variability of each wind component, as represented by its standard deviation, varies as a function of height (Fig. 4). Near all cyclones and anticyclones, the variability is greatest near the tropopause, around 9–10 km above ground level (AGL), where wind speeds tend to be greatest. In the troposphere the variability of the winds near cyclones is greater than the variability near anticyclones. While the variability in the troposphere increases monotonically with height near anticyclones, there is a relative maximum in variability around 1 km AGL near cyclones. It is likely that this relative maximum is created by variations in the structure of fronts near surface cyclones. There is a slight kink in the standard deviation profile in anticyclones around 0.5 km AGL, perhaps also owing to frontal structure. We therefore will regard the mean hodographs near anticyclones as more robust than the mean hodographs near cyclones in general and the mean hodographs near cyclones around 1 km AGL as less robust than the hodographs elsewhere in the lower half of the troposphere.

b. Composite hodographs in surface cyclones, stratified by quadrant and season

The reader is referred to Figs. 5–7 for the following discussion. The mean hodograph for all anticyclones, without regard to quadrant, is approximately the mirror image of the mean hodograph for all cyclones reflected about the axis of the meridional wind component (Fig. 5).

In the northeast quadrant of cyclones [Figs. 6 and 7 (upper right of top four panels)] winds veer strongly with height in the lowest 2–3 km owing to the effects of surface friction and warm advection. There is slight counterclockwise turning of the hodograph (i.e., of the vertical-shear vector) between approximately 2 and 8 km AGL. If the winds at these levels are approximately geostrophic, then the counterclockwise curvature must be associated with a slight backing with height of the orientation of the mean horizontal temperature gradient vector. The highest wind speeds are from the southwest, around 10 km AGL (near tropopause level), which is consistent with an upper-level trough being located to the west of the surface cyclone.

The hodograph turns sharply in a clockwise manner with height above 9 km AGL as the thermal wind reverses direction at the tropopause. Since the tropopause is typically sloped in the vicinity of baroclinic waves and troughs tend to be collocated with a relatively low tropopause, above which the air is relatively warm, there tends to be enhanced warm advection at tropopause level (Boyle and Bosart 1986). If the winds are approximately geostrophic, then veering with height and a northerly component of the thermal wind are consistent with this tropopause temperature advection pattern and are responsible for the clockwise turning of the hodograph with height near the tropopause level.

Throughout the entire depth of the troposphere and up into the lower stratosphere the winds veer with height in a pronounced manner. Thus, if the winds are nearly geostrophic, there is very deep warm advection.

The shapes of the mean hodographs in the northeast quadrant of cyclones are similar at all seasons [Figs. 6 and 7 (upper right of top four panels)]. The most pronounced differences are between summer and winter; minimum vertical shear is found during the summer. The fall and spring hodographs are similar; the spring hodograph above the planetary boundary layer (PBL), however, is rotated slightly in a counterclockwise manner with respect to the fall hodograph.

The mean hodographs in the southeast quadrant of surface cyclones [Figs. 6 and 7 (lower right of top four panels)] are qualitatively similar to those in the northeast quadrant. Very strong veering of the wind in the lowest 2–3 km is evident and is also associated with a clockwise turning of the hodograph with height. However, the hodograph becomes nearly unidirectional above 2–3 km, where there is therefore not much temperature advection (if the winds are approximately geostrophic); in the transition layer, which marks the transition from the PBL to the free atmosphere, the hodograph turns in a counterclockwise manner with height. The upper-level winds are veered from what they are in the northeast quadrant. There is sharp clockwise turning with height of the hodograph near tropopause level. The seasonal variations in the hodographs are qualitatively similar to those of the mean hodographs in the northeast quadrant of cyclones.

In the southwest quadrant of cyclones [Figs. 6 and 7 (lower left of top four panels)], in the PBL, winds veer only slightly below 1 km AGL, and back above. The absence of significant veering with height in the PBL must be due to the effect of cold advection, which is what is typically found southwest of surface cyclones, and counteracts the effect of frictional veering (Hoxit 1974). The hodograph turns sharply at 1 km AGL. There is slight clockwise hodograph curvature with height in the middle and upper troposphere and a sharp reversal in the direction of vertical shear near the tropopause. The hodograph curves much more abruptly in a clockwise manner near the tropopause during all seasons other than summer than it does in the northeast and southeast quadrants. In the summer, the hodograph curves in a clockwise manner near the tropopause [Fig. 6 (lower left of top four panels)]. The latter finding suggests that

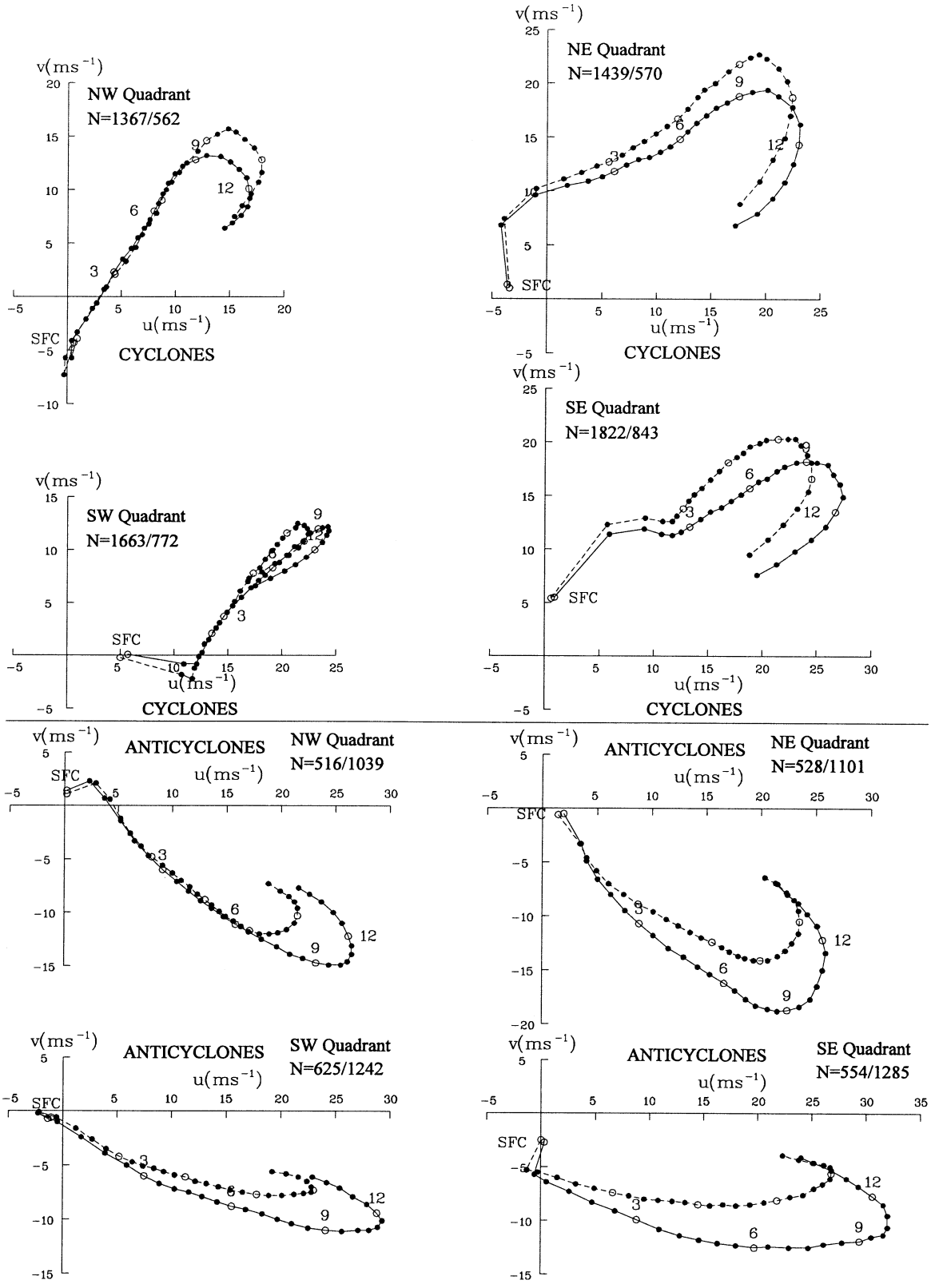

FIG. 7. As in Fig. 6 but for spring (solid line) and fall (dashed line). Spring and fall seasons are Mar–May and Sep–Nov, respectively.

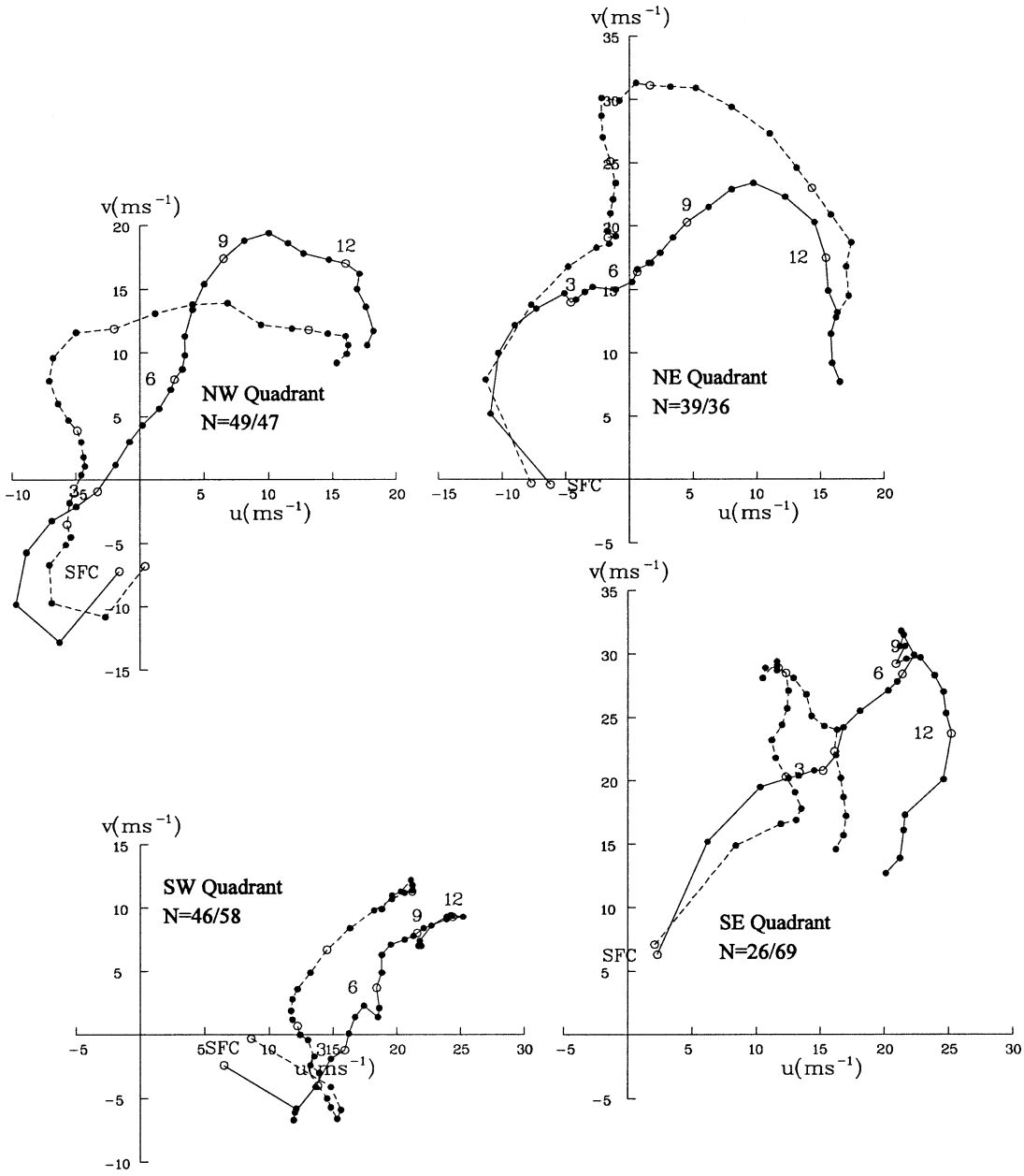

FIG. 8. As in Fig. 6 but for each quadrant of surface cyclones whose geostrophic vorticity exceeds 3f (solid line) and for surface cyclones whose minimum sea level pressure ≤980 mb (dashed line).

the vertical structure of summertime cyclones in the mean is different from that of cyclones during the other seasons; it might reflect the structure of warm-core systems such as thermal lows. For such cyclones, the upper-tropospheric flow pattern is characterized by relatively zonal flow or ridging aloft rather than a westward-sloping trough with height as in winter season baroclinic systems. Above the PBL the winds in the troposphere in a deep layer back with height, which is indicative of cold advection throughout most of the troposphere.

The most unusual aspect of the mean hodographs in the northwest quadrant of cyclones [Figs. 6 and 7 (upper left of top four panels)] is a northerly low-level jet at about 500 m AGL, which except during the summer is as strong as 7 m s^{-1}. Here we refer to a low-level jet as a local maximum in wind speed with respect to height in the lower portion of the troposphere, although it is possible there is also a local maximum in the horizontal plane, but we cannot resolve it with our compositing procedure. There might be a southerly low-level jet in the southeast sector of cyclones [Figs. 6 and 7 (lower right of top four panels)], but if it were narrower than the northerly low-level jet in the northwest quadrant, it might not be resolved in the composite. Winds generally back with height in the tro-

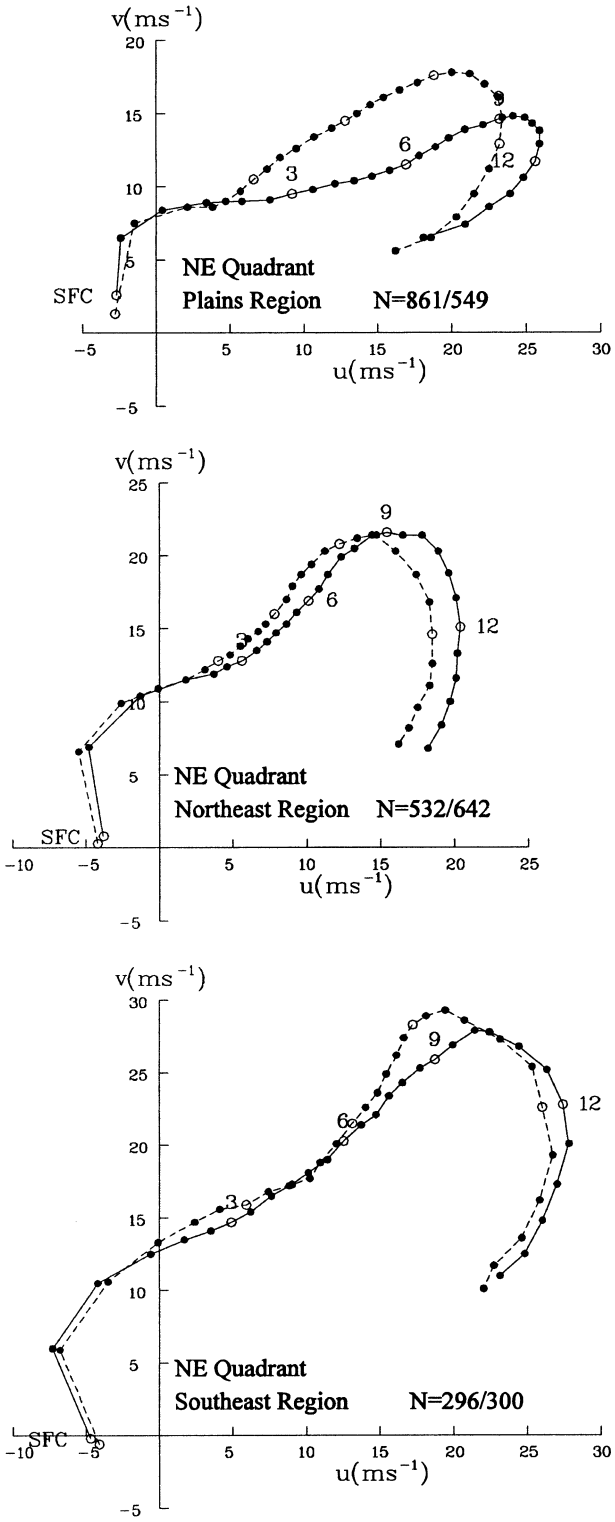

FIG. 9. As in Fig. 6 but only for the northeast quadrant of plains region, northeast region, and southeast region cyclones at 0000 (solid line) and 1200 UTC (dashed line).

posphere, which is indicative of deep cold advection, if the winds are nearly geostrophic. As in the northeast sector, there is slight counterclockwise curvature in the hodograph in the middle and upper troposphere. This feature is present only in the quadrants north of the latitude of the surface cyclone. As in the northeast and southeast quadrants, the hodograph curves in a clockwise manner near the tropopause level. Only during the summer is the curvature very sharp, as it is during all seasons in the southwest sector.

c. Composite hodographs in surface anticyclones, stratified by quadrant and season

The reader is referred to Figs. 6 and 7 for the following discussion. The mean hodographs in the northeast quadrant of surface anticyclones [Figs. 6 and 7 (upper right of bottom four panels)] are to a first approximation the mirror image of cyclones reflected about the axis of meridional wind. The wind backs with height in the lowest kilometer or so; there is therefore cold advection if the winds are approximately geostrophic. However, there is little turning of the wind with height in the troposphere above, where the winds are northwesterly and increase in speed with height; there is therefore little temperature advection above the PBL.

Unlike in cyclones [cf. Figs. 6 and 7 (upper right of top four panels)], in the northeast sector of anticyclones the hodographs turn in a counterclockwise manner with height near the tropopause, not in a clockwise manner, and the wind backs with height. This turning is probably associated with cold advection near the tropopause, since typically there is an upstream ridge and a relatively high tropopause, with relatively cold air upstream (Boyle and Bosart 1986). The counterclockwise turning of the vertical-shear vector is evident in all quadrants during all seasons. The wind speeds in the upper troposphere are greater near surface anticyclones than near cyclones, owing to the anticyclonic curvature and resulting supergeostrophic wind speed around the upper-level upstream ridge. However, the meridional component of the upper-tropospheric wind is less near surface anticyclones than near cyclones.

In the southeastern quadrant of surface anticyclones [Figs. 6 and 7 (lower right of bottom four panels)] winds veer slightly in the lowest 500 m, but back throughout the rest of the troposphere. Thus, there is a deep layer of cold advection. The hodograph curves slightly in counterclockwise manner throughout most of the troposphere. The winds and shear are strongest during the winter.

The mean hodographs in the southwest quadrant of anticyclones [Figs. 6 and 7 (lower left of bottom four panels)] exhibit a weak low-level east-northeasterly jet at about 500 m AGL, during all seasons except the summer, when it is southeasterly. The overall shapes of the hodographs are similar to those in the southeastern sector of anticyclones [Figs. 6 and 7 (lower right of bottom four panels)]. The mean hodographs during the summer, in all but the southeast sector, are rotated slight-

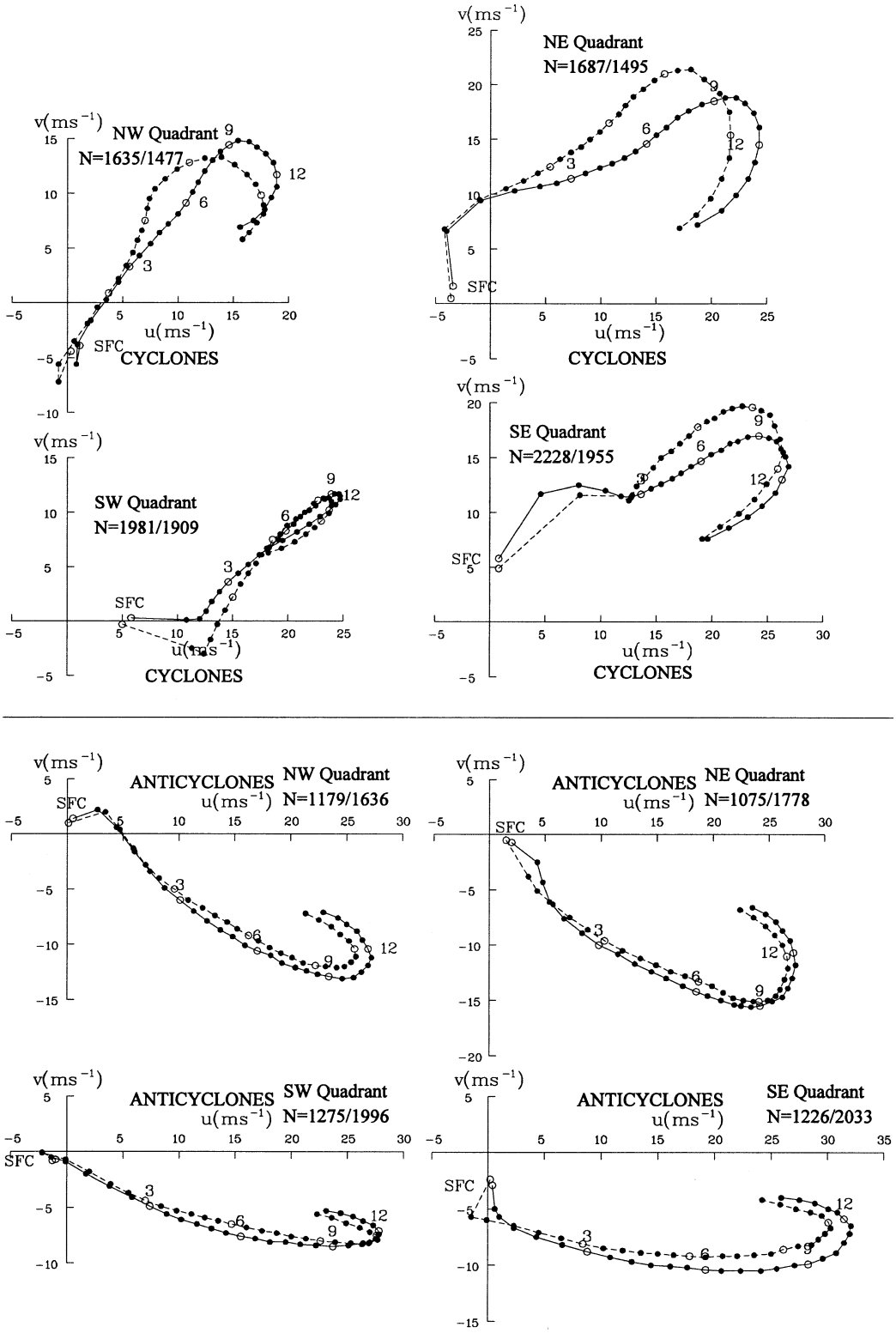

FIG. 10. As in Fig. 6 but for each quadrant of surface (top) cyclones and (bottom) anticyclones at 0000 (solid line) and 1200 UTC (dashed line).

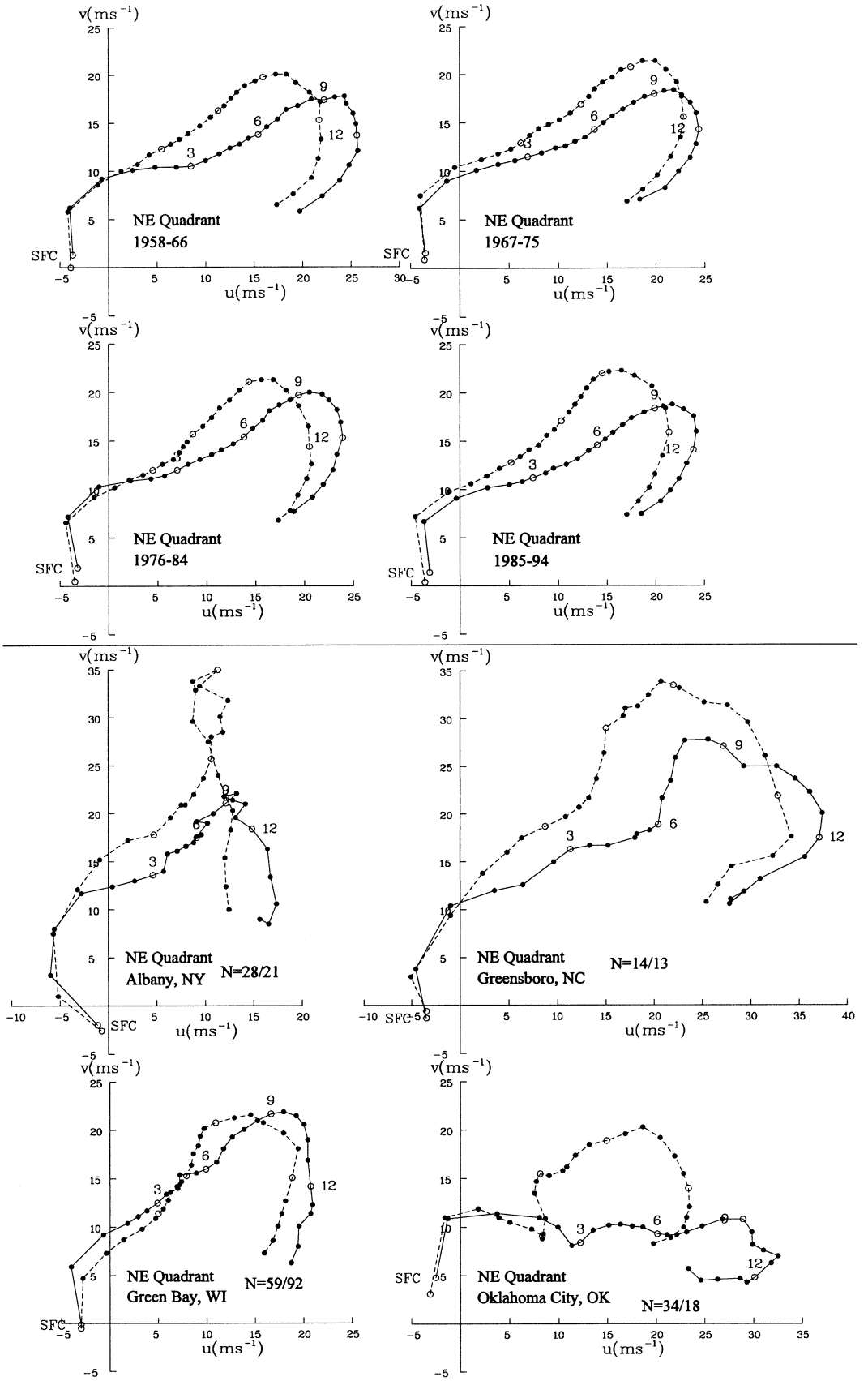
v(ms^{-1})
u(ms^{-1})
NE Quadrant
1958-66
NE Quadrant
1967-75
NE Quadrant
1976-84
NE Quadrant
1985-94
NE Quadrant
Albany, NY
N=28/21
NE Quadrant
Greensboro, NC
N=14/13
NE Quadrant
Green Bay, WI
N=59/92
NE Quadrant
Oklahoma City, OK
N=34/18
SFC
3
6
9
12

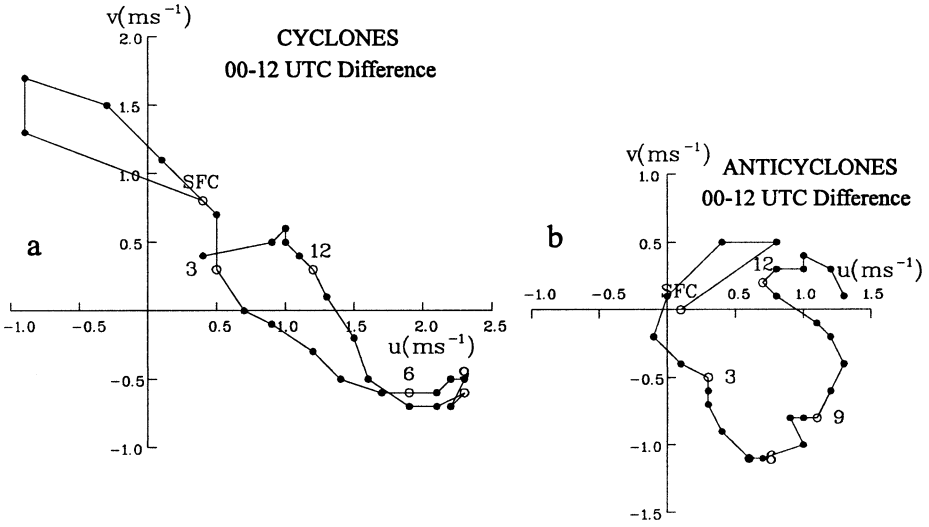

FIG. 12. Composite hodographs for the difference between the 1200 and 0000 UTC wind vectors (i.e., 0000 UTC wind vectors − 1200 UTC wind vectors) for (a) all quadrants of all cyclones and (b) all quadrants of all anticyclones.

ly in a clockwise direction from those during the other seasons; those in the northwest and southwest sectors exhibit much sharper curvature near the tropopause during the summer. However, the summer composites for anticyclones are based on the fewest samples of all the composites (Table 1) and hence must be viewed with less confidence than the others.

Veering of the wind with height in most of the troposphere is characteristic of the mean hodographs in the northwest quadrant of surface anticyclones [Figs. 6 and 7 (upper left of bottom four panels)], which is suggestive of both warm advection and, in the PBL, frictional turning. The hodographs are curved in a clockwise manner in the lowest 1 km. The summer hodograph turns sharply near the tropopause, but much more broadly during the other seasons.

d. Relative frequency of occurrence of low-level jets

Most low-level jets (local wind speed maxima with respect to height AGL) were found between 500 and 1000 m AGL. We therefore considered jets found only at or below 2000 m AGL. Altering the maximum height did not change the statistics appreciably. We computed $|\partial^2|\mathbf{v}|/\partial z^2|/|\mathbf{v}|$ to represent a measure of the normalized amplitude of the jets. It was found that for jets whose speeds were no greater than 10 m s^{-1}, most relatively high-amplitude (>0.10) jets in cyclones were located in the northwest quadrant (the northerly low-level jets); most relatively low-amplitude (<0.10) jets in cyclones were located in the southeast quadrant (the southerly low-level jets). A similar qualitative result was found for low-level jets having wind speeds in excess of 15 m s^{-1}, though there were fewer of them. The incidence of low-level jets in cyclones with wind speeds in excess of 25 m s^{-1} was too small to be considered significant.

Low-level jets were much less common near surface anticyclones than near surface cyclones. Relatively low-amplitude jets were most common in the northeast quadrant; relatively high-amplitude jets were most common in the southeast quadrant. The jets found in the northeast and southeast quadrants of anticyclones are probably associated with the northerly low-level jets found in the northwest quadrant of cyclones.

e. Composite hodographs in surface cyclones, stratified by intensity

The most intense cyclones are grouped according to the magnitude of their maximum geostrophic vorticity, with minimum thresholds of 2*f* and 3*f*, where *f* is the value of the Coriolis parameter, and with a maximum central sea level pressure threshold of 980 mb. The sample sizes for cyclones whose maximum geostrophic vorticity was in excess of 3*f* or whose minimum central sea level pressure was 980 mb or less are relatively small (Table 1); the sample sizes for cyclones whose maximum geostrophic vorticity was in excess of 2*f*, however, are more than 300 for each quadrant. These composites (not shown), therefore, do not look much different from the overall composites.

←

FIG. 11. As in Fig. 6 but only for (top) the northeast quadrant of surface cyclones by decade, and (bottom) at Albany, NY; Greensboro, NC; Green Bay, WI; and Oklahoma City, OK, at 0000 (solid line) and 1200 (dashed line) UTC.

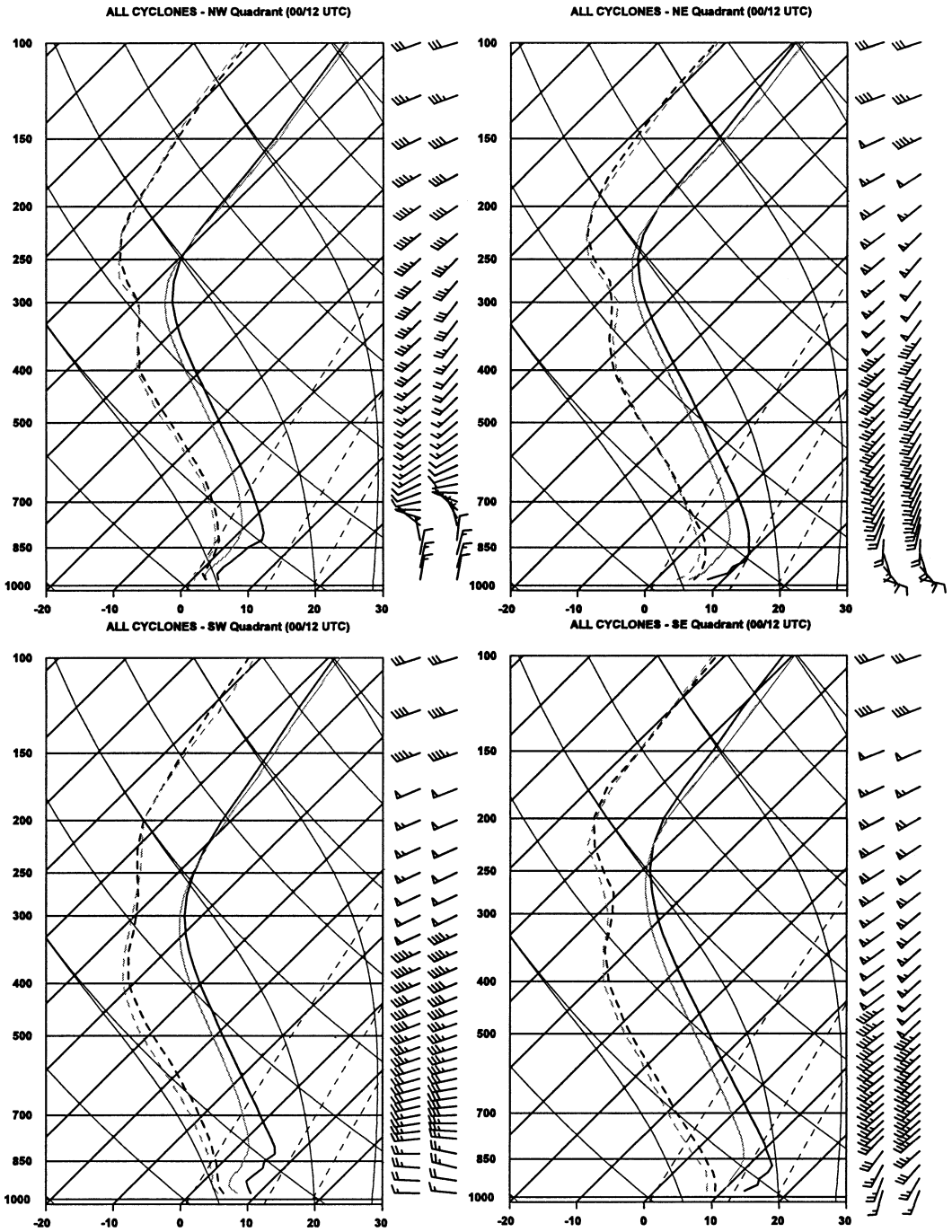

FIG. 13. Composite soundings in each quadrant of cyclones. Temperature plotted as light (dark) solid lines at 1200 (0000) UTC. Dewpoint plotted as light (dark) dashed lines at 1200 (0000) UTC. Whole (half) wind barb represents 5 (2.5) m s^{-1}. Dryadiabats, moistadiabats, and isolines of water vapor mixing ratio depicted as sloping (concave up) thin solid, sloping (concave down in bottom half, concave up in upper half) thin solid, and sloping dashed lines.

The composites for cyclones whose maximum central sea level pressure was no greater than 980 mb and the composites for cyclones whose maximum geostrophic vorticity was at least 3f are qualitatively similar (Fig. 8). We discuss the latter because it makes more sense to quantify cyclone intensity by vorticity rather than by minimum absolute pressure, since absolute pressure does not correlate as well with geostrophic wind speed around cyclones (e.g., it is possible for the pressure gradient to be relatively weak in spite of a very low absolute pressure).

The winds in the northeast and southeast quadrants

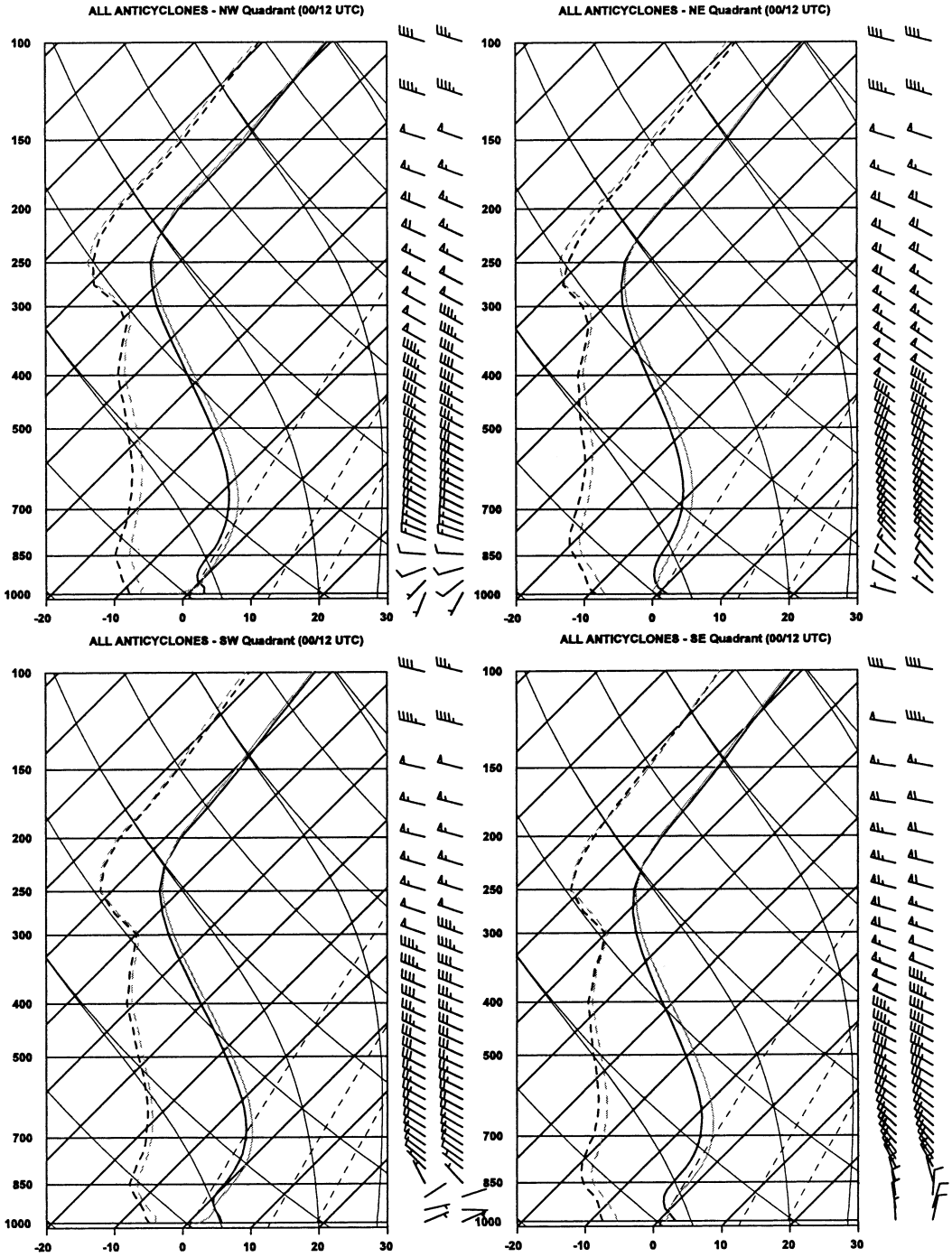

FIG. 14. As in Fig. 13 but for each quadrant of anticyclones.

of these intense cyclones are backed substantially compared to the winds in the composites for the northeast and southeast quadrant for all cyclones (cf. Figs. 5–8); this backing is reflected in a counterclockwise rotation of the hodograph, which could be a result of a higher-amplitude temperature perturbation in the baroclinic wave. However, the overall surface-to-tropopause vertical wind shear is about the same. In the southwest quadrant of the intense cyclones, the hodographs are similar to those for all cyclones, except below 3 km, where the winds are veered more to the northwest. In the northwest quadrant of the intense cyclones the hodograph is shifted in the $-u$ direction, owing to lower values of the zonal component of the wind; the low-

level jet is from the northeast and is much stronger. A low-level jet is also evident in the southwest quadrant composite of intense cyclones [Fig. 8 (bottom left of four panels)] around 1.5 km AGL. Although the sample size is relatively small compared to that for cases illustrated in Figs. 5–7, the low-level jet in the southwest quadrant of intense cyclones is significant; it is not a result of relatively few strong low-level jets that affect the mean hodograph.

f. Composite hodographs in surface cyclones, stratified by geographical region

Hodographs were also composited for the three regions indicated in Fig. 1 (inside region B). The plains region composite was intended to show the influence of the mountains to the west; the northeast region composite was intended to highlight Great Lakes cyclones and cyclones over New England; the southeast region composite was chosen to represent Gulf coast and southeastern United States coastal cyclones. Although other regional composites may make more sense and rigorous statistical techniques could be used to define better and more objectively the regions for which composites should be prepared, we arbitrarily chose the aforementioned three regions to get a preliminary feel for the geographic variation, if any, in hodograph structure. Further efforts are worthwhile, but beyond the scope of this study.

The primary difference in hodograph structure near surface cyclones (Fig. 9) is between the composite hodographs in the southeast region and those from each of the other two regions; in all quadrants the vertical shear in the troposphere is much greater in the southeast region composite. It might be that on the average the mean tropospheric baroclinicity is greatest in the southeastern region of the United States when there is a cyclone. Another notable difference in hodograph structure is found between the plains composite and each of the other two; the orientation of the mean vertical-shear vector is more zonal in the former than in the latter two. The difference in orientation might reflect a more zonally oriented baroclinic zone in the central region of the United States than in the eastern region or the effects of a zonal airstream in inducing lee cyclogenesis. Lee cyclones tend to form in the plains when the flow aloft has a westerly component, while farther east a more northeast–southwest-oriented baroclinic zone along with southwesterly flow aloft are most often associated with cyclogenesis.

The differences in hodograph structure near anticyclones (not shown) in the three different regions are not qualitatively great and therefore will not be discussed.

g. Diurnal variation of composite hodographs in surface cyclones and anticyclones, stratified by quadrant

To get an idea of how hodographs vary within each quadrant of cyclones and anticyclones as a function of time of day, we composited hodographs separately in each quadrant at 0000 and at 1200 UTC (Fig. 10). Since we were able to sample the wind profile only twice daily, we cannot determine the details of any diurnal variations. When we refer to ''diurnal variations'' we mean specifically variations between 0000 and 1200 UTC, which in the central and eastern United States are variations from early evening to early morning. There could be even stronger variations between other 12-h periods or between shorter periods.

The PBL structure in the northeast quadrant of surface cyclones [Fig. 10 (upper right of top four panels)] was nearly identical at 0000 and 1200 UTC. We suspect that in the northeast quadrant of cyclones there is often substantial cloud cover associated with ascending air in a region of warm advection; the preponderance of cloudiness limits the diurnal variability in static stability, which affects near-surface wind speed and direction (Hoxit 1974). Above 2 km AGL, however, the difference between the 0000 and 1200 UTC is marked. While the wind speeds are similar, the wind direction at 9 km AGL at 1200 UTC, for example, is backed (by 7°) with respect to the wind direction at 0000 UTC.

In the southeast quadrant of cyclones [Fig. 10 (lower right of top four panels)], above 3 km AGL, the diurnal difference in hodograph structure is similar to that in the northeast quadrant. The wind direction at 9 km AGL at 1200 UTC is backed (approximately 5°) from that at 0000 UTC. Unlike the PBL wind direction in the northeast quadrant, however, the PBL wind direction in the southeast quadrant at 0000 UTC is backed from what it is at 1200 UTC. The PBL winds may exhibit more diurnal variability in the southeast sector of cyclones owing to less cloud cover and greater diurnal variability in static stability. The diurnal variability decreases with height above the troposphere and disappears altogether by around 14 km AGL.

The most significant diurnal variations in hodograph structure in the southwest quadrant of cyclones [Fig. 10 (lower left of top four panels)] are below 3 km AGL. Above, the hodograph exhibits little 0000–1200 UTC variability. At 0000 UTC the backing of the wind with height is slightly less pronounced than it is at 1200 UTC, probably owing to lower static stability and enhanced vertical mixing at 0000 UTC.

In the northwest quadrant [Fig. 10 (upper left of top four panels)], as in the northeast and southeast quadrants, the winds above 3 km at 1200 UTC are backed (by 4°) from the winds at 0000 UTC. Below 3 km, the 0000 − 1200 UTC differences are small; the winds near the surface at 0000 UTC, however, are backed from what they are at 1200 UTC.

The differences between the 0000 and 1200 UTC composite hodographs in each quadrant of surface anticyclones are smaller overall than the differences near surface cyclones. In the southwest and northwest quadrants [Fig. 10 (lower and upper left of bottom four panels)], the 0000 − 1200 UTC differences are smallest

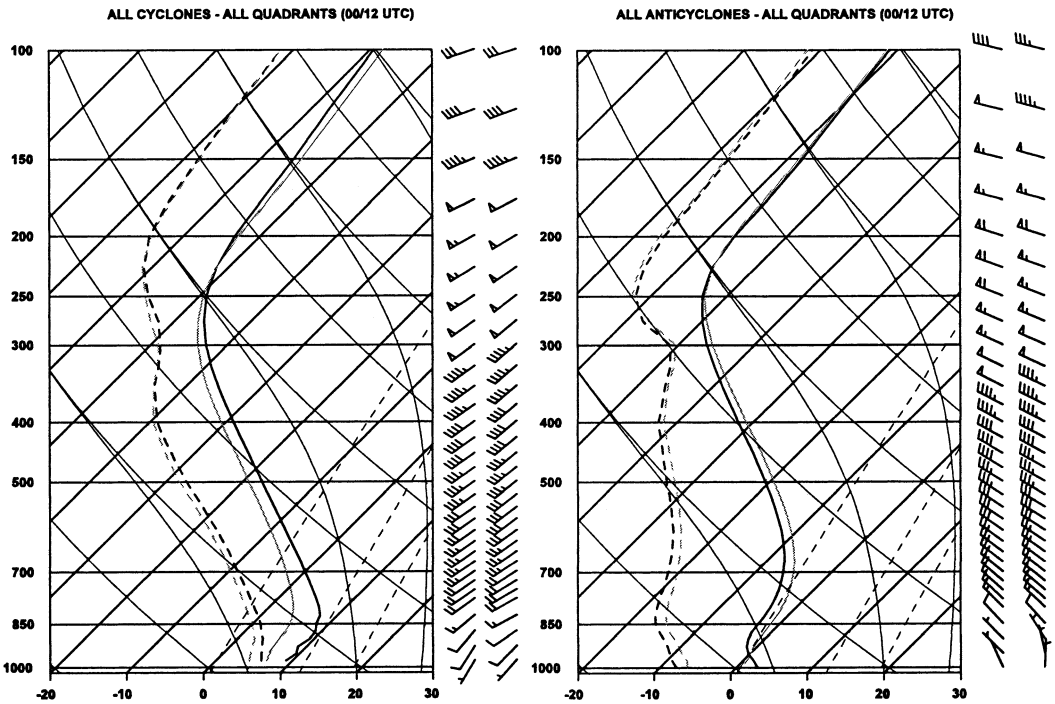

FIG. 15. As in Fig. 13 but for all quadrants in (a) cyclones and (b) anticyclones.

below 2–3 km AGL; in the northeast and southeast quadrants [Fig. 10 (upper and lower right of bottom four panels)], on the other hand, the winds in the lowest 1.5 km or so at 1200 UTC are veered noticeably from what they are at 0000 UTC. Above, the 1200 UTC wind direction is backed slightly from the wind direction at 0000 UTC.

In summary, the variations in hodograph structure, in general, between 0000 and 1200 UTC are different in the PBL from those above it. Above the boundary layer, in all but the southwest quadrant of surface cyclones, the winds back slightly at 1200 UTC from their 0000 UTC values. The diurnal variations are greater in the cyclones than in the anticyclones.

A priori, we had expected that the greatest diurnal variations would be in the PBL. To see whether the diurnal variations we documented above the boundary layer are truly representative, and not due to biases resulting from changes in equipment or sensors, or to region, we compared the diurnal differences in the quadrant-composited hodographs separately by decade, region, season, and separately for the following four long-running rawinsonde stations: Albany, New York; Green Bay, Wisconsin; Oklahoma City, Oklahoma; and Greensboro, North Carolina. For both cyclones and anticyclones it was found that the diurnal variations in hodograph structure (e.g., Fig. 11 shows variations only, for brevity, in the northeast quadrant of cyclones by decade, and at the four aforementioned sites; variations in the other quadrants and in anticyclones, etc., not shown, were similar) were indeed qualitatively consistent with our aforementioned results. The quadrant-averaged hodographs for the four rawinsonde stations, however, must be interpreted with caution since their sample sizes are relatively low and most differences in individual zonal and meridional components from 0000 to 1200 UTC did not pass a *t* test (not shown), owing to relatively large standard deviations at each level.

Diurnal variations in hodographs above the PBL have also been documented by Wallace and Hartranft (1969), who have attributed these variations in part to atmospheric tides. Although they did not composite hodographs by cyclone or anticyclone or what feature they were embedded within, they did find in part qualitatively similar overall diurnal variations (cf. their Figs. 1–5).

Lindzen (1967) has shown that the way the tidal wind vector changes with height is related to the direction of wave energy propagation in the vertical. If we use the difference between the 0000 and 1200 UTC winds as a measure of the tidal wind vector, then in cyclones it veers with height in the troposphere, above the boundary layer, and backs with height above the tropopause (Fig. 12a). In anticyclones it backs with height rapidly and through a deeper layer in the troposphere; it veers with height in the lower stratosphere (Fig. 12b). The behavior of the tidal wind vector does not deviate substantially from the overall composites when the hodographs are composited with respect to quadrant (not shown). Our results are in contrast to those of Wallace and Hartranft (1969), who, without compositing with respect to cyclones or anticyclones separately, found veering with

height in the lower stratosphere. Our result is suggestive of a downward (upward) propagation of energy in the stratosphere, and by inference a source of wave energy in the stratosphere (troposphere) near cyclones (anticyclones). Their result, on the other hand, is indicative of an overall source of wave energy in the troposphere. Since the actual behavior of the 0000 − 1200 UTC difference wind vector may be due in part to nontidal sources, it might be that these nontidal sources, which could be thermal/radiative in origin, might be dominant.

In order to compare Wallace and Hartranft's (1969) results with ours more fairly, we computed composite tidal wind hodographs for Omaha, Nebraska (cf. Fig. 12 in Wallace and Hartranft 1969), during the period from 1957 to 1994, for all cyclones, for all anticyclones, for all cyclones and anticyclones combined, and, during the 1990–92 period, for all soundings regardless of whether or not a cyclone or anticyclone was near (not shown). In both the cyclone and anticyclone composites at Omaha, the tidal wind vector backed with height in much of the troposphere and veered in the lower stratosphere, which is opposite to what we found in the cyclone composite (Fig. 12a), but identical to what we found in the anticyclone composite (Fig. 12b) and similar to what Wallace and Hartanft (1969) had found in their all-sounding composite. In the tidal wind hodograph at Omaha for all cyclones and anticyclones combined, the tidal wind vector backed with height in much of the troposphere and veered with height in the lower stratosphere. In our all-sounding composite at Omaha for the relatively short 1990–92 period, the tidal wind vector backed with height in the upper troposphere, but was difficult to determine above because its magnitude was very weak. It is therefore likely that owing to our compositing procedure with respect to cyclones and anticyclones, we have masked any variations in the diurnal variation of winds due to geographic differences.

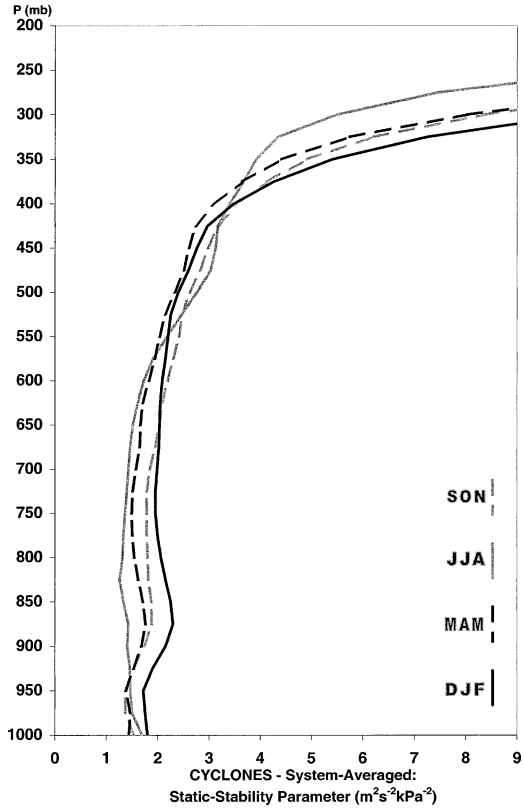

FIG. 16. Static-stability parameter (σ) as a function of pressure in (a) all quadrants and in (b) each quadrant of cyclones during the winter (dark solid line), spring (dark dashed line), summer (light solid line), and fall (light solid line).

5. Climatological analyses of thermal structure

Since the surface elevation varies across the domain, and sharp gradients (e.g., layers of high static stability or inversion layers) associated with fronts appear at different levels, the thermal structure in the composites is very much smoothed at low levels and therefore must be interpreted with caution (Brown 1993). We interpret the composite data at low levels mainly with respect to height above the ground, and mainly with respect to pressure, in the middle and upper levels of the troposphere and above.

Differences in the mean vertical distribution of temperature and dewpoint among quadrants in surface cyclones (Fig. 13) and anticyclones (Fig. 14) are greatest in the PBL. In both the northeast and southeast quadrants of cyclones there is a stable, nearly isothermal layer in the lowest 100 mb or so. In the southwest quadrant, there is a layer of relatively high lapse rate in the lowest 50 mb, surmounted by an elevated isothermal layer. In the northwest quadrant there is a shallower, low-level layer of high lapse rate surmounted by a deeper isothermal layer. In all quadrants, there is a systematic 0000 − 1200 UTC temperature difference: In the troposphere, it is on the order of several degrees Celsius warmer at 0000 than it is at 1200 UTC. The difference decreases with height and the sign of the difference reverses in the stratosphere, where the magnitude of the difference is less than it is in the troposphere. Composites by geographic region are not considered here.

In the anticyclone composites, differences are not qualitatively great among quadrants (Fig. 14). The greatest differences are between the diurnal variations of the composite for all anticyclones (Fig. 15a) and the diurnal variations of the composite for all cyclones (Fig. 15b). In anticyclones, in the troposphere the temperature at 1200 UTC is a few degrees Celsius warmer than it is at 0000 UTC, except in the lowest 50 mb. It was not expected that the daytime temperatures in much of the troposphere are warmer in the early morning in anticyclones. Since anticyclones are more frequent at 1200 UTC than at 0000 UTC, some of the difference could be due to a bias toward the 1200 UTC temperatures. The temperature in the stratosphere is cooler at 1200

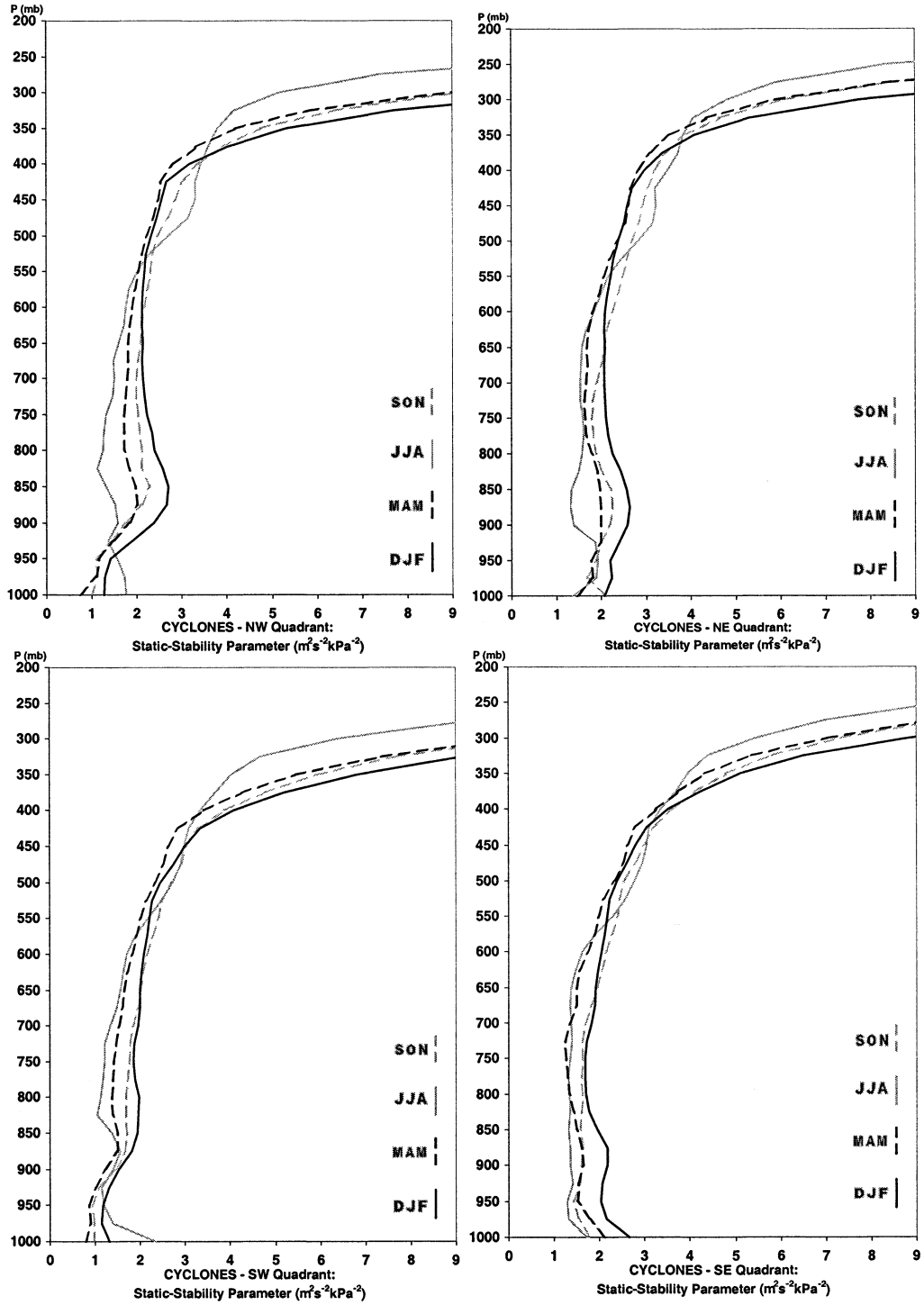

FIG. 16. (*Continued*)

UTC than it is at 0000 UTC by only a barely detectable amount. Thus, the diurnal variations in temperature in anticyclones are in the opposite sense to those in cyclones, and with smaller amplitude.

The static-stability parameter

$$\sigma = -RT/p\ \partial \ln\theta/\partial p$$

(Bluestein 1992, p. 197), a measure of the static stability often referenced in quasigeostrophic theory, is important because the forcing functions in the quasigeostroph-

ic ω equation, if held fixed, are enhanced for low values of σ and dampened by high values of σ. It is well known how the static-stability parameter increases with height in general in the troposphere and lower stratosphere. Climatological variations of σ as a function of height, by season, in cyclones and anticyclones, are not well known to the best of the authors' knowledge.

In cyclones, σ in the lower troposphere is greatest in the winter and least in the summer, except near the ground where it is least during the spring (Fig. 16a). The latter finding reflects the lingering cold air aloft from the winter season and increased insolation at the ground in the spring. In the upper troposphere it is greatest during the summer and least during the spring. In anticyclones, σ is greatest during the winter in much of the troposphere (Fig. 17a), owing to low-level cold air. Near the ground, on the other hand, it is greatest during the summer and least during the spring and winter. The latter might reflect the well-mixed conditions near shallow cold air masses behind intense surface cold fronts (e.g., Bluestein 1993, 261–262, Figs. 2.19d,e).

Differences in σ profiles in cyclones are greatest in the PBL, between the northeast and northwest quadrants, and the southeast and southwest quadrants (Fig. 16b). The static stability parameter σ mostly decreases with height in the latter two quadrants, but not in the former two. There are no significant qualitative differences by quadrant in the σ profiles for anticyclones (Fig. 17b).

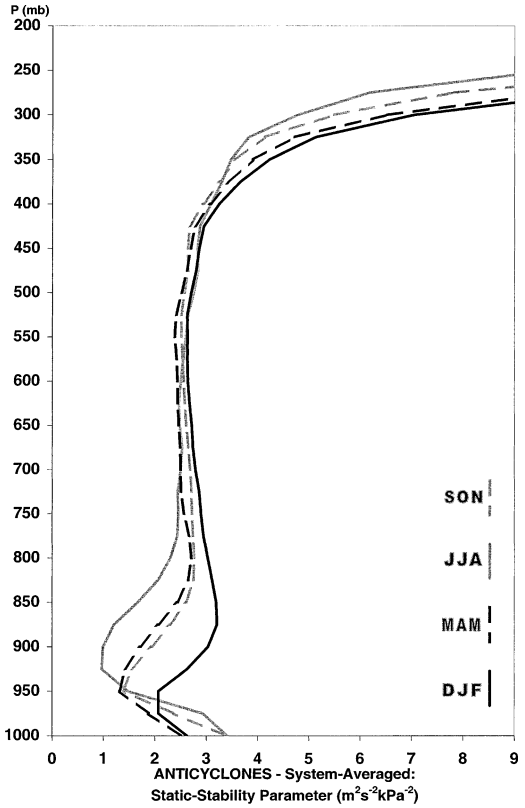

FIG. 17. As in Fig. 16 but for anticyclones.

6. Vertical cross sections of wind and potential temperature in cyclones and anticyclones

Vertical cross sections of zonal and meridional wind components and potential temperature were analyzed for the mean cyclone and for the mean anticyclone (Figs. 18–20). The plane of each cross section slices through the center of the surface cyclone or surface anticyclone. Sounding data were tabulated in 100-km range bins out to 800 km from the surface system, and were incorporated if they fell within 200 km of the plane of the cross section. Since cyclones during different portions of their life cycle are all represented in the composite, the composite represents the mean mature cyclone. However, it must be recognized, as noted earlier, that in some seasons weak cyclones are not included in the sample, while in other seasons strong cyclones are not included in the sample. Thus, the ''mean mature cyclone'' is only an approximate characterization.

East of surface cyclones, the zonal wind component increases with height and reaches a maximum around 200 mb, above which it decreases (Fig. 18). The vertical shear of the zonal wind is most intense below 800 mb (Fig. 18), which probably reflects frontal baroclinicity in the north–south direction. The thermal structure and vertical-shear cross sections are in accord with thermal wind considerations (Figs. 19 and 20). For example, the vertical shear of the zonal wind component in the top-right panel in Fig. 19 is consistent with the slope of the potential temperature isotherms in the top-left panel. Also, the vertical shear of the meridional wind component in the top-right panel in Fig. 20 is consistent with the slope of the potential temperature isotherms in the top-left panel. The zonal component of the wind is greatest about 400 km east of the center of the surface cyclone (Fig. 18) and at 225 mb equatorward of the center of the surface cyclone (Fig. 19). The zero isopleth of zonal wind component leans poleward with height out to about 400 km poleward of the cyclone center.

The meridional component of the wind is greatest at 300 mb, about 200 km east and 400 km poleward of the center of the surface cyclone (Figs. 18 and 20). The zero isopleth tilts westward with height and at 250 mb lags the 900-mb location by about 400 km. The circulation associated with the surface cyclone is separated from the upper-level trough slightly as evidenced by the relative minimum in v component east of the surface cyclone center at about 700 mb.

The zonal westerly wind component is greatest at 200 mb equatorward (Fig. 19) and east (Fig. 18) of surface anticyclones. The meridional wind component has a maximum equatorward component at 400 mb east (and

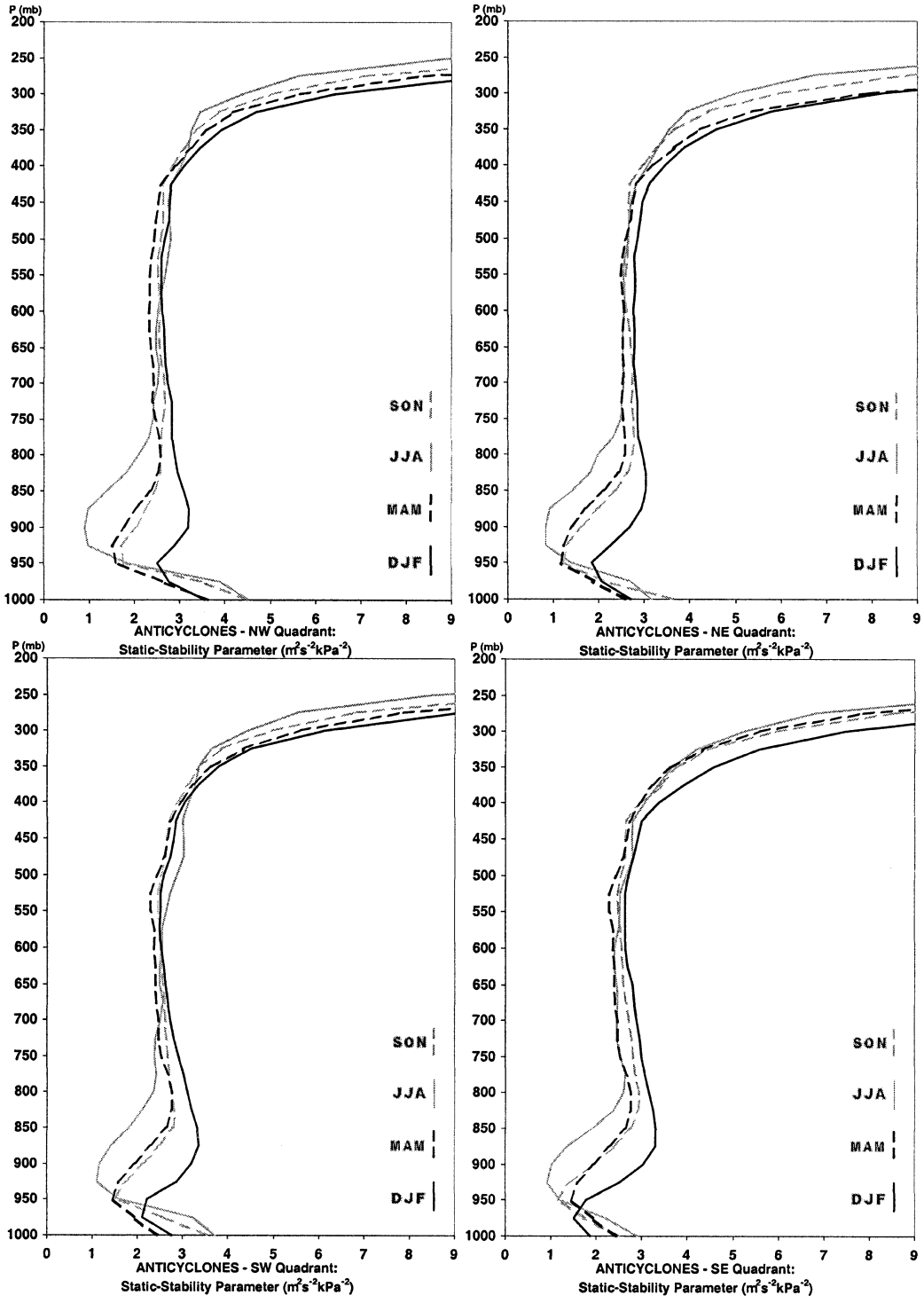

FIG. 17. (*Continued*)

at 300 mb poleward) of the center of the surface anticyclone (Figs. 20 and 18). The zero (and other) isopleth(s) of meridional wind component slope to the west with height near anticyclones more than they do near cyclones (Fig. 20).

7. Summary and discussion

The major findings from this climatological study are as follows:

1) The composite hodographs for each quadrant of cy-

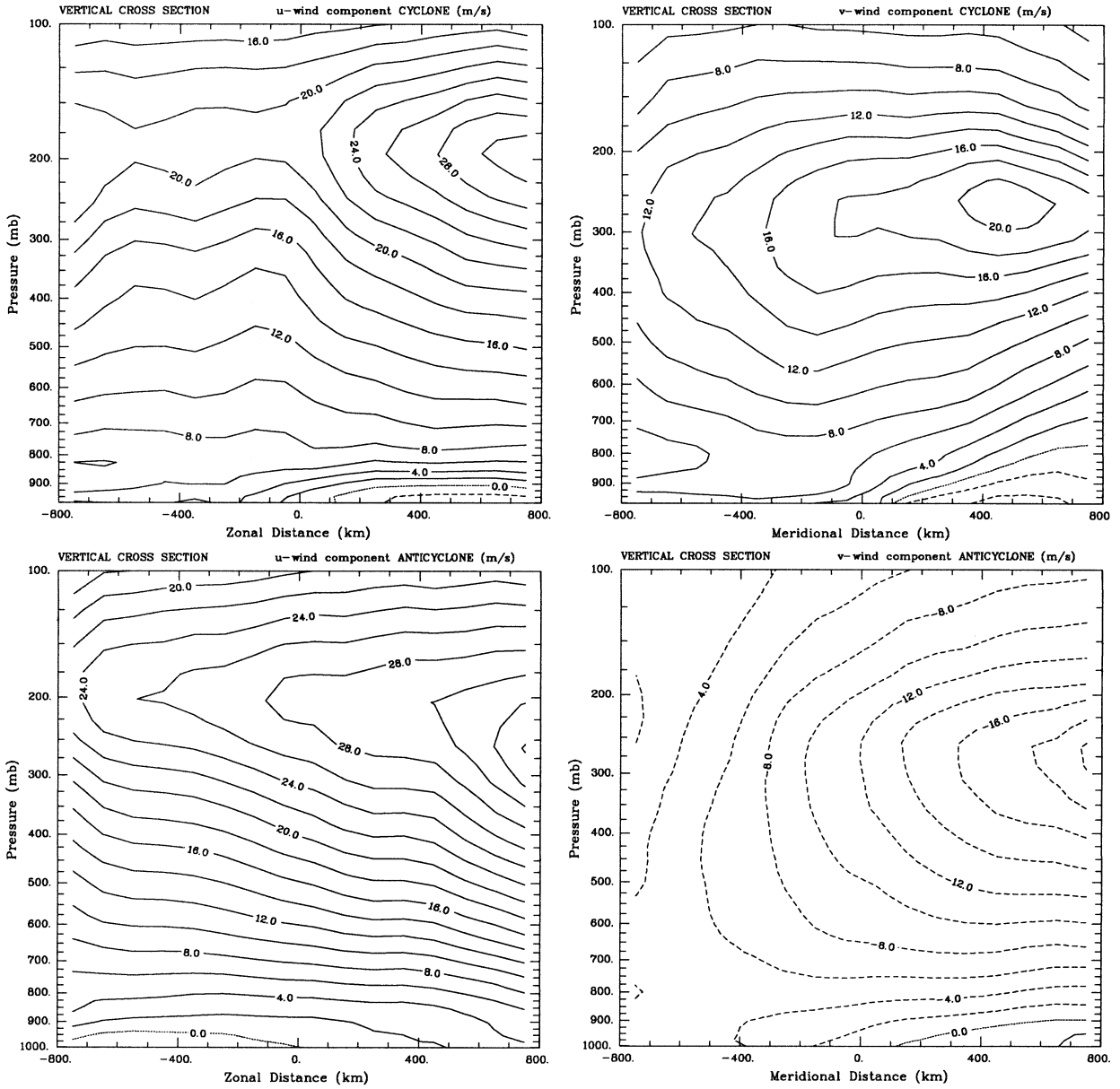

FIG. 18. Vertical cross sections through the composite of all surface cyclones meeting the objective criteria described in the main body of the text, in the eastern two-thirds of the United States, from 1 Jun 1957 to 31 Dec 1994. The origin is located at the center of the composite cyclone. The vertical coordinate is pressure. Zonal (u) component of the wind (m s^{-1}) as a function of zonal (east–west) distance from the center of the (top left) cyclones and (bottom left) anticyclones; meridional (v) component of the wind (m s^{-1}) as a function of meridional (north–south) distance from the center of (top right) cyclones and (bottom right) anticyclones. Solid (dashed) contours indicate positive (negative) values. Positive (negative) distance is measured poleward (equatorward) or east of (west of) the cyclone/anticyclone centers.

clones and anticyclones are significantly different and may be attributed to the unique structure, in the mean, of synoptic-scale baroclinic waves in midlatitudes.

2) There is, in general, a diurnal variation in hodograph structure: In all but the southwest quadrant of cyclones and in all quadrants of anticyclones, there is a counterclockwise rotation of the mean hodograph between 0000 and 1200 UTC, that is, between early evening and early morning. The effect is greater in cyclones than in anticyclones, and varies quantitatively with quadrant.
3) An equatorward-directed low-level jet appears, in the mean, in the northwest quadrant of surface cyclones. Low-level jets do not appear, in the mean, in any other quadrant of cyclones or in anticyclones.
4) The composite hodographs near the tropopause, in cyclones, turn in a clockwise direction with height,

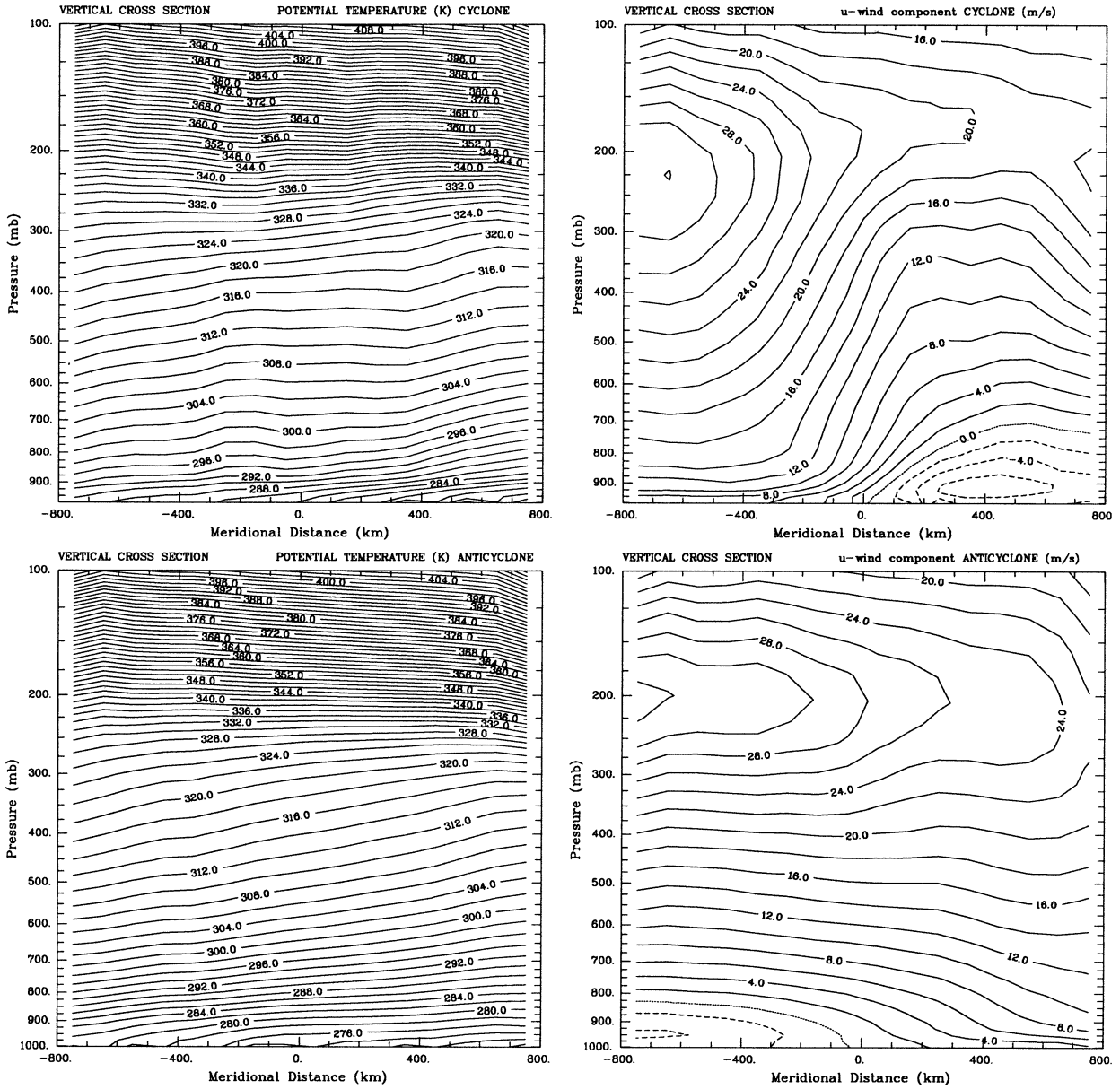

FIG. 19. As in Fig. 18 but for potential temperature (K) as a function of meridional distance from the center of (top left) cyclones and (bottom left) anticyclones. Zonal component of the wind as a function of meridional distance from the center of (top right) cyclones and (bottom right) anticyclones.

while those in anticyclones turn in a counterclockwise direction with height. This behavior can be explained in terms of the temperature structure and the temperature advection pattern near the tropopause, which slopes between upper-level troughs and downstream ridges.

The first major finding can be used to see how well a given hodograph conforms to that for the mean baroclinic wave and to estimate the expected mean structure of embedded mesoscale precipitation systems, if they are initiated. The composite hodographs can serve as standards to which specific hodographs can be compared.

The composite hodographs in the northeast and southeast sectors of cyclones are characteristic of the environments of cyclonically rotating, right-moving supercells (e.g., Weisman and Klemp 1982, 1984; Bluestein and Jain 1985) in that the mean 0–6-km shear is at least 20 m s^{-1} and the hodograph has some clockwise curvature in the lower troposphere. In the southeast quadrant, but not in the northeast quadrant, there is a relative minimum in shear at 1.5–3 km AGL (Brown 1993). It is not known what significant dynamical consequences,

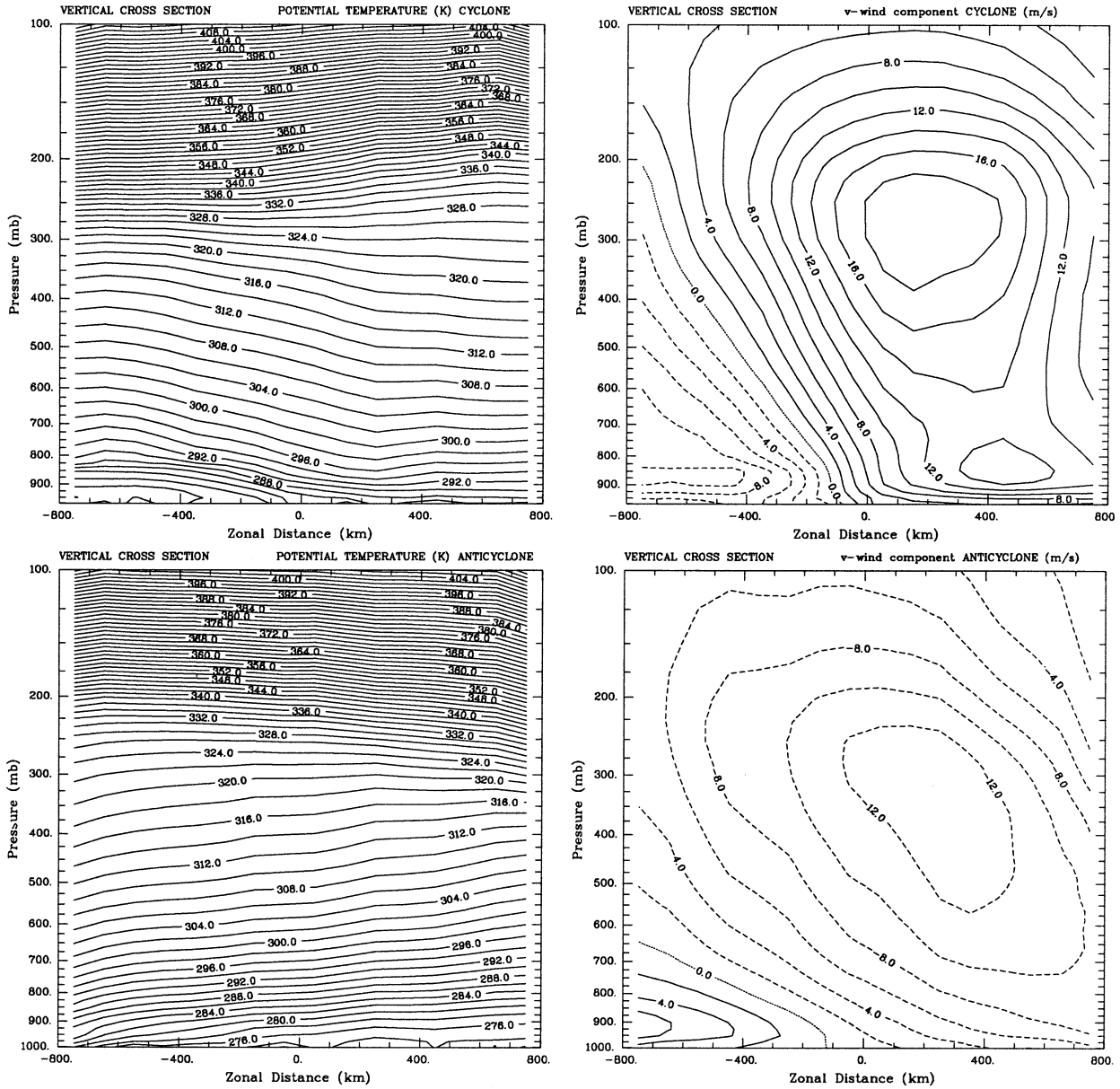

FIG. 20. As in Fig. 18 but for potential temperature as a function of zonal distance from the center of (top left) cyclones and (bottom left) anticyclones. Meridional component of the wind as a function of zonal distance from the center of (top right) cyclones and (bottom right) anticyclones.

if any, this minimum in low- to midlevel shear has; they could be explored using numerical experiments. In the southwest quadrant of cyclones, the shear is also strong enough for supercells, which, owing to the counterclockwise kink at 1 km, would support left-moving, anticyclonically rotating supercells. However, convective storms tend not to be triggered in this quadrant, which typically is located behind a surface cold front. Similarly, the mean hodograph in the northwest sector of cyclones also can support supercells, but the northwest sector of cyclones is also not a location where intense convective development takes place.

Since winter season bands of precipitation associated with conditional symmetrical instability (CSI) should line up, in the mean, with the midlevel thermal wind shear vector, in the northeast quadrant of cyclones, where the necessary conditions for CSI are sometimes present (Wolfsberg et al. 1986), southwest–northeast-oriented bands should predominate if the shear is representative of the geostrophic (thermal wind) shear.

The composite hodographs in the northeast and southeast quadrants of anticyclones are conducive for the formation of anticyclonic, left-moving supercells, owing to the large shear and counterclockwise curvature with

height. However, it is unlikely that these sectors would support intense-storm development, owing to the low-level cold advection present in the northerly or northwesterly low-level flow. However, in the southwest and northwest sectors of anticyclones the hodographs are supportive in general of cyclonically, right-moving supercells, owing to low-level clockwise curvature with height and high shear; these are regions where one might expect intense-storm development can occur. The southwest quadrant of surface anticyclones is a more likely environment for the formation of intense convective storms just east of the Rocky Mountains, where the low-level flow transports relatively high values of moisture upslope (Doswell 1980).

The second major finding, the diurnal variation in hodographs above the PBL, has not, we believe, been appreciated very much by the community at large, and needs further explanation and study, especially with radar wind profilers, which can provide wind data with much higher temporal resolution than the observational rawinsonde network. From rawinsonde observations made only twice daily, it is not possible to determine the diurnal or semidiurnal components of the tide owing to aliasing.

Two possible explanations for the diurnal variation in hodographs are that (a) it is a result of atmospheric tidal oscillations (Wallace and Hartranft 1969; Hsu and Hoskins 1989; Whiteman and Bian 1996; Chen et al. 1998) and (b) that is a result of radiative-thermal processes; the latter two effects could be modified by topography. Since its character is different in cyclones and anticyclones, it cannot be purely tidal in nature, since tides should be dependent mainly on location and time, not on the atmospheric flow pattern. Factors that might influence the diurnal variation are differences in radiation, which are functions of cloudiness and water vapor content (Wallace and Hartranft 1969); cloudiness and water vapor content vary as a function of location with respect to cyclones and anticyclones (Carlson 1980). Also, differences in latent heat release, which also vary as a function of location, might be important. It is noteworthy that diurnal variations in temperature also appear in the composited soundings and vary depending on whether or not they are in a cyclone or anticyclone, and in which quadrant they appear. The diurnal variations in hodograph and temperature are documented independently. These variations in hodograph and temperature need to be investigated further from a theoretical standpoint. In addition, the variations need to be documented further in composites subdivided by geographical region and time of year.

The third major finding, the documentation of the mean, equatorward-directed low-level jet (in a region of sharp backing of the wind with height) in the northwest quadrant of cyclones, underscores the ubiquity of strong cold advection in the PBL northwest of cyclones. The low-level poleward directed jet, which does not show up in our composites east of the cyclone, has been discussed extensively in the literature, while the equatorward-directed low-level jet, which does show up in our composites, has not. Perhaps it is time that this feature be studied and documented further.

While the fourth major finding, the mirror-image behavior in the curvature of hodographs near the tropopause, can be explained relatively easily, it remains to be seen if it has any significance for the structure of precipitation systems in the troposphere. For relatively shallow systems that do not reach up to the tropopause, the curvature of the hodograph at the tropopause likely has no effect. For deep convective storms, however, it might affect the dynamics and kinematics of anvils and of penetrating tops.

This study has been limited to the eastern two-thirds of the United States. It should be extended to include, if possible, other regions of the world. Composites of cyclone and anticyclone structure could be done for finer subclasses of cyclones and anticyclones. For example, composites of lee cyclones, Alberta clippers, etc. might harbor interesting findings. Composites computed from the NCEP–NCAR reanalysis dataset should be considered as an alternative to use of the actual data. Inferences about the mean hodograph structure in cyclones and anticyclones over data-sparse areas such as over the ocean would then be possible.

Finally, the relative contributions of the geostrophic and ageostrophic wind components to the hodographs should be determined. Use of an analytical model such as that which Sanders (1971) has used (Banacos 1999) has demonstrated that the ageostrophic wind in some quadrants of cyclones and anticyclones can be a significant fraction of the total wind.

Acknowledgments. We are grateful to Fred Carr [University of Oklahoma (OU)] and Mike Richman (OU) for their stimulating extended discussions as members of the second author's master's thesis committee. Ed Bracken (University of Albany), Tom Yoksas (UNIDATA), David Dowell (OU), Rafal Jabrzemski (OU), Greg Lehmiller (OU), Chris Weiss (OU), and Tom Condo (OU) provided substantial computing assistance. Chuck Doswell III (NSSL), Lance Bosart (University of Albany), and Kerry Emanuel (MIT) generously shared their views and ideas. Bob Johns at the Storm Prediction Center provided an informal review. Dennis Joseph (NCAR) provided information about the navy analyses. Pat Pauley (NRL) is acknowledged for her review and for her efforts in providing additional documentation of the sea level pressure data. This work was supported by the School of Meteorology at OU and in part by NSF Grants ATM-9612674 and ATM-991209.

REFERENCES

Baker, N. L., 1992: Quality control for the navy operational atmospheric database. *Wea. Forecasting,* **7,** 250–261.

Banacos, P. C., 1999: The wind and thermal structure surrounding

synoptic-scale cyclones and anticyclones over the eastern two-thirds of the United States: A climatological analysis. M.S. thesis, School of Meteorology, University of Oklahoma, 221 pp. [Available from School of Meteorology, University of Oklahoma, 100 E. Boyd, Rm. 1310, Norman, OK 73019.]

Barker, E., 1992: Design of the navy's multivariate optimum interpolation analysis system. *Wea. Forecasting,* **7,** 220–231.

Barnes, S. L., 1964: A technique for maximizing details in numerical weather map analysis. *J. Appl. Meteor.,* **3,** 396–409.

Bluestein, H. B., 1992: *Principles of Kinematics and Dynamics.* Vol. I. *Synoptic–Dynamic Meteorology in Midlatitudes,* Oxford University Press, 431 pp.

——, 1993: *Observations and Theory of Weather Systems.* Vol. II. *Synoptic–Dynamic Meteorology in Midlatitudes,* Oxford University Press, 594 pp.

——, and M. H. Jain, 1985: Formation of mesoscale lines of precipitation: Severe squall lines in Oklahoma during the spring. *J. Atmos. Sci.,* **42,** 1711–1732.

Bosart, L. F., 1990: Degradation of the North American radiosonde network. *Wea. Forecasting,* **5,** 527–528.

Boyle, J. S., and L. F. Bosart, 1986: Cyclone–anticyclone couplets over North America. Part II: Analysis of a major cyclone event over the eastern United States. *Mon. Wea. Rev.,* **114,** 2432–2465.

Brown, R. A., 1993: A compositing approach for preserving significant features in atmospheric profiles. *Mon. Wea. Rev.,* **121,** 874–880.

Carlson, T. N., 1980: Airflow through midlatitude cyclones and the comma cloud pattern. *Mon. Wea. Rev.,* **108,** 1498–1509.

Carr, F. H., and J. P. Millard, 1985: A composite study of comma clouds and their association with severe weather over the Great Plains. *Mon. Wea. Rev.,* **113,** 370–387.

Changnon, D., J. J. Noel, and L. H. Maze, 1995: Determining cyclone frequencies using equal-area circles. *Mon. Wea. Rev.,* **123,** 2285–2294.

Chen, T.-C., M.-C. Yen, and R. W. Arritt, 1998: Detection of semidiurnal wind oscillations with a radar profiler. *Bull. Amer. Meteor. Soc.,* **79,** 1921–1924.

Collins, W. G., and L. S. Gandin, 1990: Comprehensive hydrostatic quality control at the National Meteorological Center. *Mon. Wea. Rev.,* **118,** 2752–2767.

Dey, C. H., 1989: The evolution of objective analysis methodology at the National Meteorological Center. *Wea. Forecasting,* **4,** 297–312.

Dickinson, M. J., L. F. Bosart, W. E. Bracken, G. J. Hakim, D. M. Schultz, M. A. Bedrick, and K. R. Tyle, 1997: The March 1993 superstorm cyclogenesis: Incipient phase synoptic- and convective-scale flow interaction and model performance. *Mon. Wea. Rev.,* **125,** 3041–3072.

Doswell, C. A., III, 1980: Synoptic-scale environments associated with high plains severe thunderstorms. *Bull. Amer. Meteor. Soc.,* **61,** 1388–1400.

Elliott, W. P., and D. J. Gaffen, 1991: The utility of radiosonde humidity archives for climate studies. *Bull. Amer. Meteor. Soc.,* **72,** 1507–1520.

Friedman, M., 1972: New radiosonde case: Problem and solution. *Bull. Amer. Meteor. Soc.,* **53,** 884–887.

Gandin, L. S., 1988: Complex quality control of meteorological observations. *Mon. Wea. Rev.,* **116,** 1138–1156.

Goerss, J. S., and P. A. Phoebus, 1992: The navy's operational atmospheric analysis. *Wea. Forecasting,* **7,** 232–249.

Hoxit, L. R., 1974: Planetary boundary layer winds in baroclinic conditions. *J. Atmos. Sci.,* **31,** 1003–1020.

Hsu, H.-H., and B. J. Hoskins, 1989: Tidal fluctuations as seen in ECMWF data. *Quart. J. Roy. Meteor. Soc.,* **115,** 247–264.

Kalnay, E., and Coauthors, 1996: The NCEP/NCAR 40-Year Reanalysis Project. *Bull. Amer. Meteor. Soc.,* **77,** 437–471.

Koch, S. E., M. DesJardins, and P. J. Kocin, 1983: An interactive Barnes objective map analysis scheme for use with satellite and conventional data. *J. Climate Appl. Meteor.,* **22,** 1487–1503.

Lindzen, R. S., 1967: Thermally driven diurnal tide in the atmosphere. *Quart. J. Roy. Meteor. Soc.,* **93,** 18–42.

Maddox, R. A., 1976: An evaluation of tornado proximity wind and stability data. *Mon. Wea. Rev.,* **104,** 133–142.

Mass, C., 1993: The application of compact disks (CD-ROM) in the atmospheric sciences and related fields: An update. *Bull. Amer. Meteor. Soc.,* **74,** 1901–1908.

——, H. J. Edmon, H. J. Friedman, N. R. Cheney, and E. E. Recker, 1987: The use of compact discs for the storage of large meteorological and oceanographic data sets. *Bull. Amer. Meteor. Soc.,* **68,** 1556–1558.

Petterssen, S., 1956: *Motion and Motion Systems.* Vol. I. *Weather Analysis and Forecasting,* McGraw-Hill, 428 pp.

Pratt, R. W., 1985: Review of radiosonde temperature and humidity problems. *J. Atmos. Oceanic Technol.,* **2,** 404–407.

Rosmond, T. E., 1992: The design and testing of the Navy Operational Global Atmospheric Prediction System. *Wea. Forecasting,* **7,** 262–272.

Rotunno, R., and J. B. Klemp, 1982: The influence of the shear-induced pressure gradient on thunderstorm motion. *Mon. Wea. Rev.,* **110,** 136–151.

——, and ——, 1985: On the rotation and propagation of simulated supercell thunderstorms. *J. Atmos. Sci.,* **42,** 271–292.

Sanders, F., 1971: Analytic solutions of the nonlinear omega and vorticity equations for a structurally simple model of disturbances in the baroclinic westerlies. *Mon. Wea. Rev.,* **99,** 393–408.

——, and J. R. Gyakum, 1980: Synoptic–dynamic climatology of the ''bomb.'' *Mon. Wea. Rev.,* **108,** 1589–1606.

Schaefer, J. T., and C. A. Doswell III, 1979: On the interpolation of a vector field. *Mon. Wea. Rev.,* **107,** 458–476.

Schultz, D. M., and P. N. Schumacher, 1999: The use and misuse of conditional symmetric instability. *Mon. Wea. Rev.,* **127,** 2709–2732.

Schwartz, B. E., 1990: Regarding the automation of rawinsonde observations. *Wea. Forecasting,* **5,** 167–171.

——, and C. A. Doswell III, 1991: North American rawinsonde observations: Problems, concerns, and a call to action. *Bull. Amer. Meteor. Soc.,* **72,** 1885–1896.

Sinclair, M. R., 1994: An objective cyclone climatology for the Southern Hemisphere. *Mon. Wea. Rev.,* **122,** 2239–2256.

Taljaard, J. J., 1967: Development, distribution, and movement of cyclones and anticyclones in the Southern Hemisphere during the IGY. *J. Appl. Meteor.,* **6,** 973–987.

Taylor, K. E., 1986: An analysis of the biases in traditional cyclone frequency maps. *Mon. Wea. Rev.,* **114,** 1481–1490.

Wallace, J. M., and F. R. Hartranft, 1969: Diurnal wind variations, surface to 30 kilometers. *Mon. Wea. Rev.,* **97,** 446–455.

Weisman, M. L., and J. B. Klemp, 1982: The dependence of numerically simulated convective storms on vertical wind shear and buoyancy. *Mon. Wea. Rev.,* **110,** 504–520.

——, and ——, 1984: The structure and classification of numerically simulated convective storms in directionally varying wind shears. *Mon. Wea. Rev.,* **112,** 2479–2498.

Whiteman, C. D., and X. Bian, 1996: Solar semidiurnal tides in the troposphere: Detection by radar profilers. *Bull. Amer. Meteor. Soc.,* **77,** 529–542.

Whittaker, L. M., and L. H. Horn, 1984: Northern Hemispheric extratropical cyclone activity for four mid-season months. *J. Climatol.,* **4,** 297–310.

Wolfsberg, D. G., K. A. Emanuel, and R. E. Passarelli, 1986: Band formation in a New England winter storm. *Mon. Wea. Rev.,* **114,** 1552–1569.

Zishka, K. M., and P. J. Smith, 1980: The climatology of cyclones and anticyclones over North America and surrounding ocean environs for January and July 1950–77. *Mon. Wea. Rev.,* **108,** 387–401.